SUPPORTING INFORMATION

Effect of the heteroatom on the magnetic and luminescent properties of hybrid lanthanide-substituted Keggin-type polyoxometalates

Janire Bustamante-Fernández,[a,b] Estibaliz Ruiz-Bilbao,[b] Corina Rodríguez-Esteban,[b] Mathieu Gonidec,[c] José A. Garcia,[d] Luis Lezama,[a] Juan M. Gutiérrez-Zorrilla[a,b], Itziar Oyarzabal,[b,e,*] and Beñat Artetxe[a,*]

[a]Departamento de Química Orgánica e Inorgánica, Facultad de Ciencia y Tecnología, Universidad del País Vasco UPV/EHU, P.O. Box 644, 48080 Bilbao, Spain. benat.artetxe@ehu.eus
[b]BCMaterials, Edificio Martina Casiano, 3rd Floor, UPV/EHU Science Park, Barrio Sarriena s/n, 48940 Leioa, Spain. itziar.oyarzabal@bcmaterials.net
[c]Univ. Bordeaux, CNRS, Bordeaux INP, ICMCB, UMR 5026, F-33600 Pessac, France.
[d]Departamento de Física Aplicada II, Facultad de Ciencia y Tecnología. Universidad del País Vasco UPV/EHU, P.O. Box 644, 48080 Bilbao, Spain.
[e]IKERBASQUE, Basque Foundation for Science, 48009 Bilbao, Spain.

Table of Contents

Materials and Methods

The monolacunary Keggin-type $K_8[\alpha\text{-}GeW_{11}O_{39}]\cdot 13H_2O$ precursor[1] and the N,N'-dimethyl-N,N'-bis(2-hydroxy-3-formyl-5-bromobenzyl)ethylenediamine (H_2L) ligand[2] were synthetized following the reported procedures and afterwards identified by means of Fourier transformed infrared (FT-IR) spectroscopy and ^{1}H-NMR, respectively. All chemicals were obtained from commercial sources and used without further purification. The C, H and N content of all the compounds was determined on a PerkinElmer 2400 CHN analyzer. FT-IR spectra were obtained on a Shimadzu FTIR-8400S spectrometer as KBr pellets. Powder X-ray diffraction (PXRD) patterns were collected from 2θ = 5 to 50° (0.03° step size, 30 s per step) using a Philips X'PERT PRO diffractometer operating at 40 kV/40 mA in θ–θ configuration with monochromated Cu Kα radiation (λ = 1.5418 Å) and a PIXcel detector. Diffuse reflectance UV/Vis spectra were registered for crystalline samples using a double beam UV-Vis-NIR Agilent Cary 7000 spectrometer equipped with an integration sphere (Internal DRA 900).

Variable-temperature magnetic susceptibility, magnetization and alternating-current (*ac*) susceptibility measurements were carried out with PPMS (Physical Property measurement System) – Model 6000, MPMS 7XL SQUID and MPMS3 SQUID magnetometers. Diamagnetic corrections were estimated from the Pascal's constants. *Ac* measurements were performed with an oscillating magnetic field of 3.5 Oe. The optimum external field (H_{dc} = 2500 Oe for **1_{Ge}-Gd**; H_{dc} = 1000 Oe for **1_{Ge}-Dy** and **1_{Ge}-Yb**) was determined from field-dependent measurements. The samples were measured by both X-band (Bruker ELEXSYS 500 system, super-high-Q resonator ER-4123-SHQ) and Q-band (Bruker EMX system, ER-510-QT resonator) continuous wave EPR spectrometers. The magnetic field was calibrated by NMR probes and the frequency inside the cavities was determined with integrated MW-frequency counters. Data were collected and processed using the Bruker X_{EPR} suite. Photoluminescence (PL) emission spectra were recorded for single crystals of **1_{Ge}-Ln** (Ln = Sm to Lu) samples from 10 K to room temperature using a close cycle helium cryostat contained in an Edinburgh Instruments FLS920 spectrometer equipped with a Müller-elektronik- Optik SVX1450 Xe lamp and a Kimmon IK3552R-G He:Cd continuous laser (325 nm). The lifetime measurements were performed using a μF1 pulsed microsecond flashlamp as an excitation source. Photographs of bulky samples were taken in a micro-PL system included in an Olympus optical microscope (Color View III camera) illuminated with a Hg lamp. The overall quantum yield (%) was measured in the solid state for **1_{Ge}-Eu** and **1_{Ge}-Sm** using a Horiba Quanta–φ integrating sphere equipped with an Oriel Instruments MS257 lamp as excitation source and an Horiba iHR550 spectrometer to analyse the emission.

General Synthetic Procedure

A mixture of 5 mL MeOH containing the H_2L ligand (0.051 g, 0.1 mmol) and the corresponding lanthanide salt (0.1 mmol) was added dropwise to a solution of $K_8[\alpha\text{-}GeW_{11}O_{39}]\cdot 13H_2O$ precursor (0.326 g, 0.1 mmol) dissolved in 25 mL of 0.5M aqueous KAc/HAc buffer (pH = 4.6) at 100°C. The resulting solution was heated for 1 hour, filtered and left to evaporate at room temperature in an open container. Powders generated in 12h were filtered off and yellow single-crystals of $K_5[Ln^{III}(\alpha\text{-}GeW_{11}O_{39})(H_2L)]\cdot 14H_2O$ (Ln^{III} = Sm to Lu, **1_{Ge}-Ln**; $H_2L = C_{20}H_{22}Br_2N_2O_4$) were obtained from the resulting clear solutions in less than one week.

$K_5[Sm(\alpha\text{-}GeW_{11}O_{39})(C_{20}H_{22}Br_2N_2O_4)]\cdot 14H_2O$ (1_{Ge}-Sm). $Sm(NO_3)_3\cdot 6H_2O$ (0.044 g) was used as the 4f metal source. Yield: 19 mg, 5% based on W. IR, $\tilde{\nu}$ = 1626 (s), 1539 (m), 1452 (m), 1425 (w), 1383 (w), 1304 (w), 1230 (w), 1203 (w), 1163 (w), 1020 (w), 947 (s), 879 (vs), 808 (vs), 744 (vs), 704 (s), 509 (m). Elem Anal. calcd (%) for $C_{20}H_{50}Br_2GeK_5N_2O_{57}SmW_{11}$: C, 6.27%; H, 1.32%; N, 0.73%. Found: C, 6.41 %; H,1.42 %; N, 0.71 %.

$K_5[Eu(\alpha\text{-}GeW_{11}O_{39})(C_{20}H_{22}Br_2N_2O_4)]\cdot 14H_2O$ (1_{Ge}-Eu). $Eu(NO_3)_3\cdot 6H_2O$ (0.045 g) was used as the 4f metal source. Yield: 20 mg, 5% based on W. IR, $\tilde{\nu}$ = 1628 (s), 1541 (m), 1454 (m), 1425 (w), 1383 (w), 1313 (w), 1232 (w), 1205 (w), 1163 (w), 1020 (w), 945 (s), 877 (vs), 810 (vs), 744 (s), 706 (s), 511 (m). Elem Anal. calcd (%) for $C_{20}H_{50}Br_2EuGeK_5N_2O_{57}W_{11}$: C, 6.27%; H, 1.31%; N, 0.73%. Found: C, 6.50%; H, 1.66%; N, 0.76%.

$K_5[Gd(\alpha\text{-}GeW_{11}O_{39})(C_{20}H_{22}Br_2N_2O_4)]\cdot 14H_2O$ (1_{Ge}-Gd). $Gd(NO_3)_3\cdot 6H_2O$ (0.045 g) was used as the 4f metal source. Yield: 26 mg, 6% based on W. IR, $\tilde{\nu}$ = 1626 (s), 1541 (m), 1456 (m), 1425 (w), 1383 (w), 1309 (w), 1232 (w), 1203 (w), 1163 (w), 1020 (w), 949 (s), 877 (vs), 810 (vs), 746 (s), 704 (s), 507 (m). Elem Anal. calcd (%) for $C_{20}H_{50}Br_2GeGdK_5N_2O_{57}W_{11}$: C, 6.26%; H, 1.31%; N, 0.73%. Found: C, 6.39 %; H, 1.47 %; N, 0.75 %.

$K_5[Tb(\alpha\text{-}GeW_{11}O_{39})(C_{20}H_{22}Br_2N_2O_4)]\cdot 14H_2O$ (1_{Ge}-Tb). $Tb(NO_3)_3\cdot 5H_2O$ (0.044 g) was used as the 4f metal source. Yield: 21 mg, 5% based on W. IR, $\tilde{\nu}$ = 1628 (vs), 1539 (m), 1456 (m), 1425 (w), 1383 (w), 1306 (w), 1232 (w), 1205 (w), 1165 (w), 1020 (w), 949 (s), 879 (vs), 814 (vs), 746 (s), 706 (s), 509 (m). Elem Anal. calcd (%) for $C_{20}H_{50}Br_2GeK_5N_2O_{57}TbW_{11}$: C, 6.26%; H, 1.31%; N, 0.73%. Found: C, 6.68%; H, 1.56%; N, 0.83%.

$K_5[Dy(\alpha\text{-}GeW_{11}O_{39})(C_{20}H_{22}Br_2N_2O_4)]\cdot 14H_2O$ ($\mathbf{1_{Ge}}$-Dy). $Dy(NO_3)_3\cdot 6H_2O$ (0.046 g) was used as the 4f metal source. Yield: 20 mg, 5% based on W. IR, $\tilde{\nu}$ = 1630 (s), 1539 (m), 1456 (m), 1427 (w), 1385 (m), 1306 (w), 1232 (w), 1205 (m), 1165 (w), 1022 (w), 947 (s), 881 (vs), 814 (vs), 746 (s), 706 (s), 511 (m). Elem Anal. calcd (%) for $C_{20}H_{50}Br_2DyGeK_5N_2O_{57}W_{11}$: C, 6.25%; H, 1.31%; N, 0.73%. Found: C, 6.33%; H, 1.67%; N, 0.78%.

$K_5[Ho(\alpha\text{-}GeW_{11}O_{39})(C_{20}H_{22}Br_2N_2O_4)]\cdot 14H_2O$ ($\mathbf{1_{Ge}}$-Ho). $Ho(NO_3)_3\cdot 5H_2O$ (0.044 g) was used as the 4f metal source. Yield: 24 mg, 6% based on W. IR, $\tilde{\nu}$ = 1626 (s), 1539 (m), 1456 (m), 1425 (w), 1383 (w), 1304 (w), 1232 (w), 1205 (m), 1165 (w), 1022 (m), 949 (s), 879 (vs), 814 (vs), 746 (s), 706 (s), 511 (m). Elem Anal. calcd (%) for $C_{20}H_{50}Br_2GeHoK_5N_2O_{57}W_{11}$: C, 6.25%; H, 1.31%; N, 0.73%. Found: C, 6.43 %; H, 1.39 %; N, 0.74 %.

$K_5[Er(\alpha\text{-}GeW_{11}O_{39})(C_{20}H_{22}Br_2N_2O_4)]\cdot 14H_2O$ ($\mathbf{1_{Ge}}$-Er). $Er(NO_3)_3\cdot 5H_2O$ (0.044 g) was used as the 4f metal source. Yield: 26 mg, 5% based on W. IR, $\tilde{\nu}$ = 1628 (vs), 1539 (m), 1458 (m), 1425 (w), 1383 (w), 1306 (w), 1232 (w), 1205 (w), 1165 (w), 1022 (w), 947 (s), 879 (vs), 814 (vs), 748 (s), 706 (s), 513 (m). Elem Anal. calcd (%) for $C_{20}H_{50}Br_2ErGeK_5N_2O_{57}W_{11}$: C, 6.24%; H, 1.31%; N, 0.73%. Found: C, 6.71%; H, 1.77%; N, 0.84%.

$K_5[Tm(\alpha\text{-}GeW_{11}O_{39})(C_{20}H_{22}Br_2N_2O_4)]\cdot 14H_2O$ ($\mathbf{1_{Ge}}$-Tm). $Tm(NO_3)_3\cdot 5H_2O$ (0.045 g) was used as the 4f metal source. Yield: 20 mg, 5% based on W. IR, $\tilde{\nu}$ = 1630 (vs), 1541 (m), 1458 (m), 1425 (w), 1383 (w), 1304 (w), 1232 (w), 1205 (w), 1165 (w), 1024 (w), 947 (s), 879 (vs), 816 (vs), 748 (s), 708 (s), 509 (m). Elem Anal. calcd (%) for $C_{20}H_{50}Br_2GeK_5N_2O_{57}TmW_{11}$: C, 6.24%; H, 1.31%; N, 0.73%. Found: C, 6.22%; H, 1.62%; N, 0.80%.

$K_5[Yb(\alpha\text{-}GeW_{11}O_{39})(C_{20}H_{22}Br_2N_2O_4)]\cdot 14H_2O$ ($\mathbf{1_{Ge}}$-Yb). $Yb(NO_3)_3\cdot 5H_2O$ (0.045 g) was used as the 4f metal source. Yield: 5 mg, 1% based on W. IR, $\tilde{\nu}$ = 1632 (s), 1537 (m), 1458 (m), 1425 (w), 1381 (w), 1313 (w), 1277 (w), 1205 (w), 1167 (w), 1020 (m), 945 (s), 876 (vs), 816 (vs), 748 (s), 708 (s), 511 (m). Elem Anal. calcd (%) for $C_{20}H_{50}Br_2GeK_5N_2O_{57}W_{11}Yb$: C, 6.23%; H, 1.31%; N, 0.73%. Found: C, 6.31 %; H, 1.33 %; N, 0.74 %.

$K_5[Lu(\alpha\text{-}GeW_{11}O_{39})(C_{20}H_{22}Br_2N_2O_4)]\cdot 14H_2O$ ($\mathbf{1_{Ge}}$-Lu). $Lu(NO_3)_3\cdot 5H_2O$ (0.046 g) was used as the 4f metal source. Yield: 1 mg, <1% based on W. IR, $\tilde{\nu}$ = 1631 (s), 1537 (m), 1457 (m), 1426 (w), 1381 (w), 1309 (w), 1275 (w), 1206 (w), 1166 (w), 1020 (m), 945 (s), 875 (vs), 816 (vs), 749 (s), 709 (s), 512 (m). Elem Anal. calcd (%) for $C_{20}H_{50}Br_2GeK_5N_2O_{57}W_{11}Yb$: C, 6.23%; H, 1.31%; N, 0.73%. Found: C, 6.29 %; H, 1.32 %; N, 0.74 %.

Thermal Analyses

Thermogravimetric and differential thermal analyses (TGA/DTA) were carried out from room temperature to 800°C on a Mettler Toledo TGA/SDTA851^e thermobalance at a rate of 5 °C min^{-1} and under a 50 cm^3min^{-1} flow of synthetic air (Figure S1 and Table S1). Prior to the analysis, solid crystalline samples were filtered from mother solutions and left to dry overnight. Thermal decomposition of **$\mathbf{1_{Ge}}$-Ln** occurs via two distinct stages. The endothermic dehydration process extends from room temperature up to *ca.* 150 °C. In all cases, the presence of 14 hydration molecules per molecular formula of **$\mathbf{1_{Ge}}$-Ln** were estimated. The second stage is an exothermic process associated with the combustion of the organic ligand and it is accompanied by the breakdown of the POM framework. Finally, the final residues obtained at temperatures in the 660–720 °C range correspond to two major phases identified by powder X-ray diffraction (Figure S2): the hexagonal P63/*mcm* $K_{0.33}W_{0.94}O_3$ (PDF: 01-081-0005)[3] and monoclinic C2/*c* $KLn(WO_4)_2$ (Ln = Sm to Lu; PDF for Ln = Dy: 00-023-0479).[4]

Table S1. Thermal data for compounds **$\mathbf{1_{Ge}}$-Ln**.

	Dehydration (Δm, %)		Decomposition (°C)	Residue (m, %)	
	Δm_{calc} for $14H_2O$	Δm_{exp}	T_d	Calc. for $K_5LnGeO_{39}W_{11}$	Exp.
$\mathbf{1_{Ge}}$-Sm	6.6	6.6	682	21.0	22.2
$\mathbf{1_{Ge}}$-Eu	6.6	6.6	720	20.9	22.2
$\mathbf{1_{Ge}}$-Gd	6.6	6.0	670	20.9	22.9
$\mathbf{1_{Ge}}$-Tb	6.6	6.0	718	20.9	21.4
$\mathbf{1_{Ge}}$-Dy	6.6	6.4	669	20.9	22.7
$\mathbf{1_{Ge}}$-Ho	6.6	6.1	670	20.9	21.9
$\mathbf{1_{Ge}}$-Er	6.6	5.6	660	20.9	21.8
$\mathbf{1_{Ge}}$-Tm	6.6	6.0	705	20.8	20.8
$\mathbf{1_{Ge}}$-Yb	6.5	6.5	675	20.8	23.8
$\mathbf{1_{Ge}}$-Lu	6.5	6.0	655	20.8	21.4

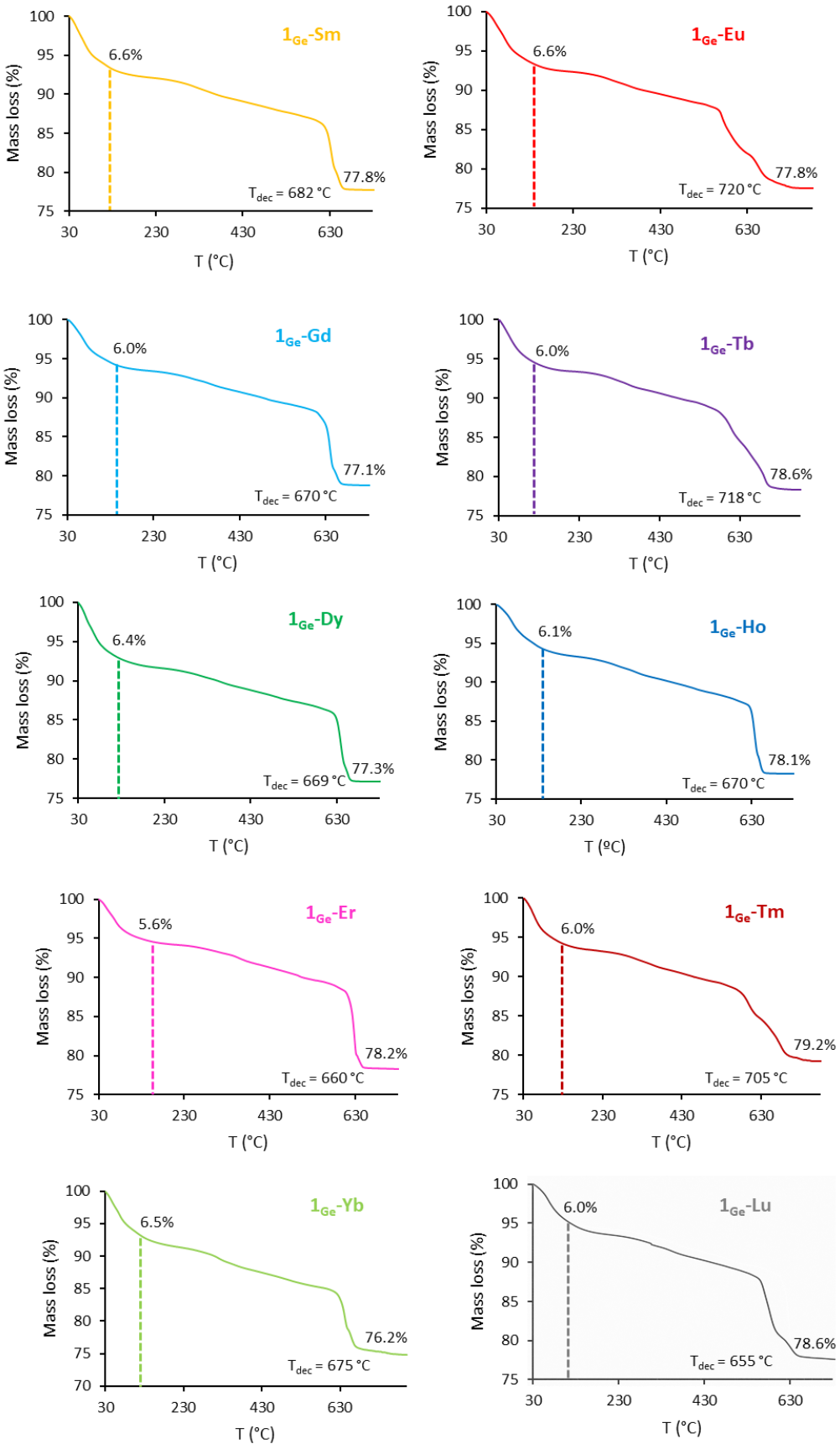

Figure S1. TGA curves of compounds **1_{Ge}-Ln** (Ln = Sm to Lu).

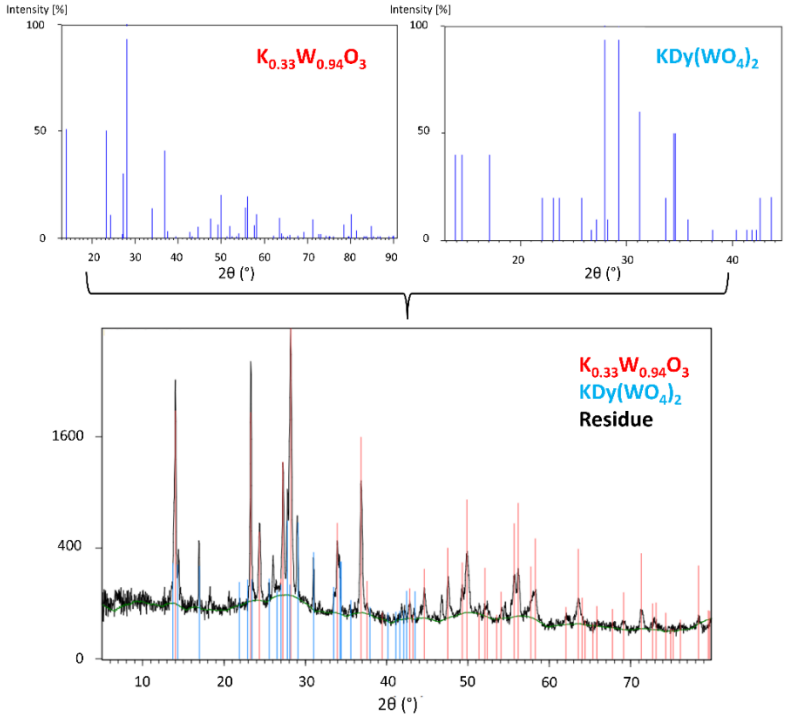

Figure S2. Identification of the final residue from the thermal decomposition of **1_{Ge}-Dy** by PXRD analyses, as a representative example of the **1_{Ge}-Ln** family.

FT-IR Spectroscopy and Powder X-Ray Diffraction

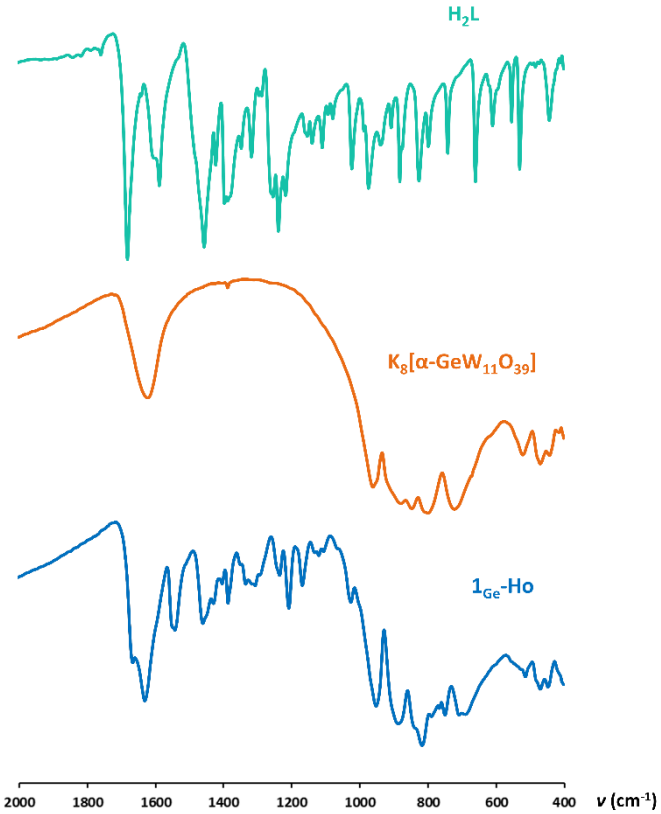

Figure S3. FT-IR spectra of **1_{Ge}-Ho** in comparison to the those of the starting materials (The H_2L ligand, and the $K_8[\alpha\text{-}GeW_{11}O_{39}]\cdot 13H_2O$ POM precursor).

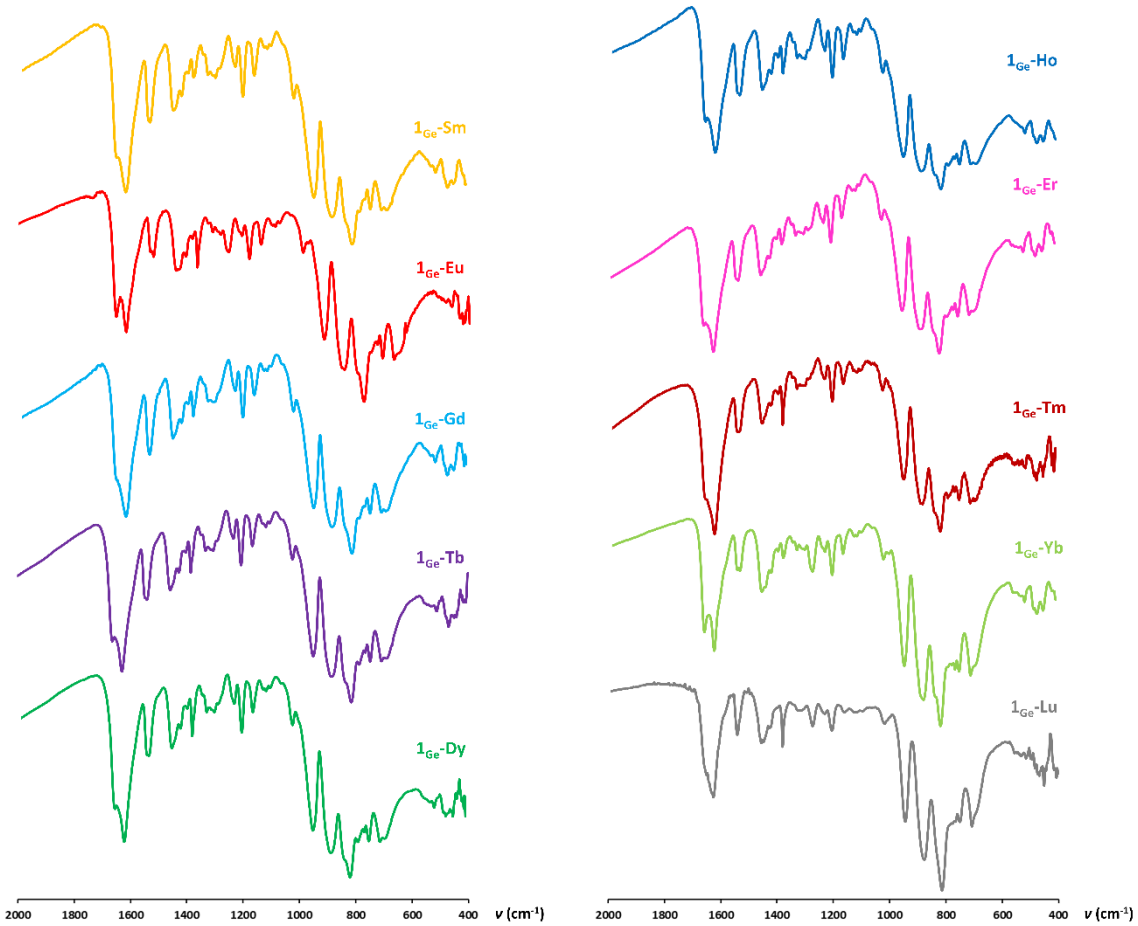

Figure S4. FT-IR spectra of **1_{Ge}-Ln** (Ln = Sm to Lu).

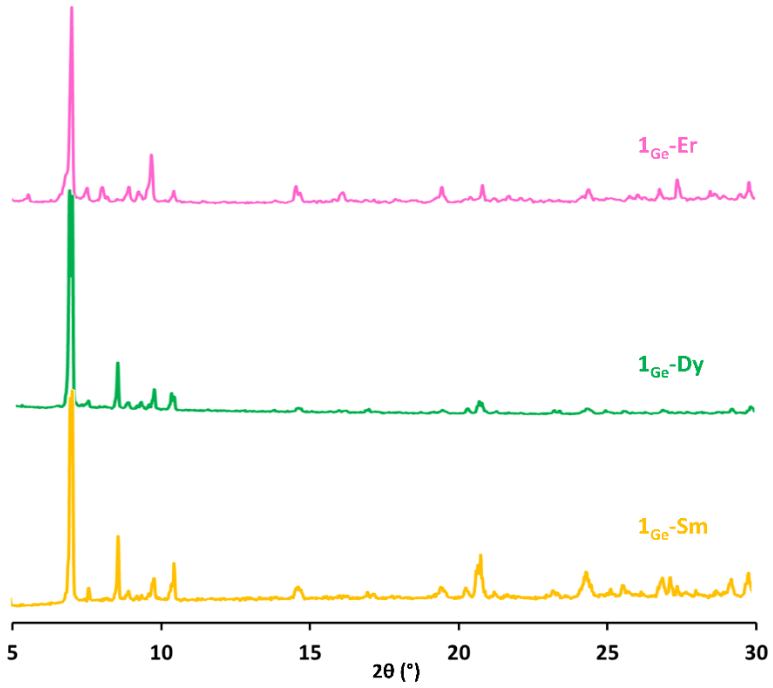

Figure S5. Experimental powder X-ray diffraction patterns of the freshly filtered crystals.

Single Crystal X-Ray Diffraction

Crystallographic data for compounds **1_{Ge}-Ln** (Ln = Sm to Lu) are provided in Table S2. Intensity data were collected at 170.00(10) K on an Agilent Technologies SuperNova Diffractometer equipped with monochromated Mo Kα radiation (λ = 0.71073 Å) and a HyPix (Hybrid Pixel Array) detector for all **1_{Ge}-Ln** (Ln = Sm – Tm and Lu) except for **1_{Ge}-Yb** that was recorded at 150.01(10) K and an Eos CCD detector. Data frames (unit cell determination, Gaussian absorption correction with face indexing, intensity data integration, and correction for Lorentz and polarization effects) were processed using CrysAlis Pro software package.[5] The structures were solved using OLEX2[6] program and refined by full-matrix least-squares with SHELXL-2018/3.[7] Final geometrical calculations were carried out with PLATON[8] as integrated in WinGX.[9] Visualization of the structures was performed with Crystal-Maker,[10] whereas SHAPE was employed to perform continuous shape measurements.[11]

Thermal vibrations were treated anisotropically for heavy atoms (W, Ln, Br, Ge and K) as well as for O_{POM} atoms except in Eu and Yb derivatives. Hydrogen atoms of the organic H_2L ligands were placed in calculated positions and refined using SHELXL parameters. Some of the anisotropic thermal ellipsoids from some potassium cations and O_{POM} atoms were normalized using ISOR-type restrains from SHELXL, as well as in some carbon atoms from the H_2L ligand and some Br atoms in the compounds **1_{Ge}-Gd** and **1_{Ge}-Tm**, respectively. In a similar way, some O_{POM}–O_W bond lengths were normalized using DFIX and hydrogen atoms from the H_2L ligand with DANG-type command. All compounds display significant disorder between potassium counterions and lattice hydration water molecules. This prevents us from modelling all the cation/solvent network. Thus, only 12 to 18 sites with appropriate geometries for K cations were located in Fourier maps. These occupancies were initially refined without restrictions and fixed to the first decimal in the last cycle, which results in a total number between 9.3 (**1_{Ge}-Lu**) to 12.3 (**1_{Ge}-Tb**) potassium atoms per each asymmetric unit containing three hybrid polyanions. Analogously, only 33 to 72 positions suitable for water molecules were determined in the crystal structures of **1_{Ge}-Ln**. Due to this disorder, large solvent accessible voids can be found in the final structures, which account for 12 to 29% of the unit cell volume. According to PLATON, the largest voids are located at (i) x, y, z = 0, 0.5, 0 and occupy a volume of 2414 (**1_{Ge}-Dy**), 1960 (**1_{Ge}-Ho**), 1793 (**1_{Ge}-Tm**) and 3206 Å^3 (**1_{Ge}-Lu**); (ii) x, y, z = 0, 0, 0 occupying a volume of 3957 (**1_{Ge}-Eu**), 1596 (**1_{Ge}-Tb**) and 2869 (**1_{Ge}-Yb**); (iii) x, y, z = 0, 1, 0.5 occupying a volume of 3205 Å^3 (**1_{Ge}-Sm**); (iv) x, y, z = 0, 0.5, 0.5 and occupy a total volume of 2236 Å^3 (**1_{Ge}-Gd**); (v) x, y, z = -0.5, 0, 0 occupying a volume of 1600 Å^3 (**1_{Ge}-Er**). Elemental and thermal analyses (Table S1, Figure S1) were essential to unequivocally determine the presence of 15 K ions and 42 hydration water molecules, that correspond to five K^+ and 14 water molecules per formula which could be well located in these structural voids. It is worth noting that the presence of methanol solvent molecules was dismissed on the basis of elemental analyses. Finally, all the structures exhibit large maxima of residual electron density, located close to the W atoms as indicated by the final difference density map. This large residual maxima in the final Fourier map is common in the refinement of polyoxotungstate structures due to the high level of absorption of heavy atoms such as W.

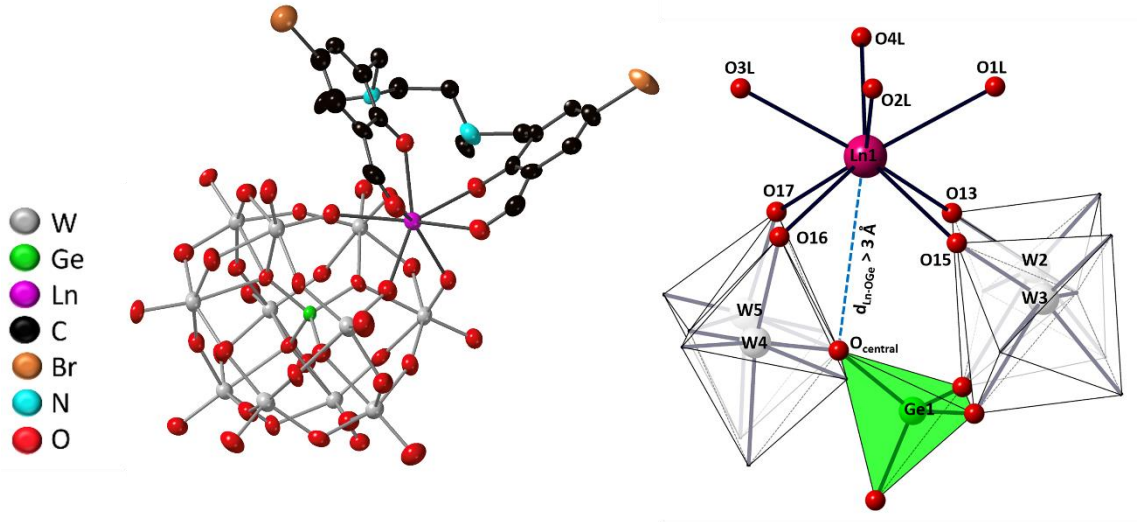

Figure S6. Left: ORTEP view of the hybrid molecular $[Dy(H_2L)(\alpha\text{-}GeW_{11}O_{39})]^{5-}$ anion in **1_{Ge}-Dy** showing 50% probability displacement ellipsoids. Right: Scheme of the coordination spheres of the Ln centres in **1_{Ge}-Ln**.

Table S2. Crystallographic data for **1_{Ge}-Ln** (Ln = Sm–Lu).

	1_{Ge}-Sm	**1_{Ge}-Eu**	**1_{Ge}-Gd**	**1_{Ge}-Tb**	**1_{Ge}-Dy**
empirical formula	$C_{20}H_{50}Br_2GeK_5N_2O_{57}SmW_{11}$	$C_{20}H_{50}Br_2EuGeK_5N_2O_{57}W_{11}$	$C_{20}H_{50}Br_2GdGeK_5N_2O_{57}W_{11}$	$C_{20}H_{50}Br_2GeK_5N_2O_{57}TbW_{11}$	$C_{20}H_{50}Br_2DyGeK_5N_2O_{57}W_{11}$
fw ($g \cdot mol^{-1}$)	3831.23	3832.84	3838.13	3839.80	3843.38
crystal system	triclinic	triclinic	triclinic	triclinic	triclinic
space group (number)	$P\bar{1}$ (2)	$P\bar{1}$ (2)	$P\bar{1}$ (2)	$P\bar{1}$ (2)	$P\bar{1}$ (2)
a (Å)	21.9100(3)	21.8651(3)	21.7822(2)	21.8750(3)	21.8276(3)
b (Å)	24.7934(3)	24.8167(4)	24.7260(3)	24.7768(4)	24.7948(4)
c (Å)	28.5204(4)	28.5375(5)	28.2514(3)	28.4883(4)	28.4816(4)
α (°)	113.2344(11)	113.2874(15)	113.9823(11)	113.1772(13)	113.2727(13)
β (°)	95.5495(10)	95.4668(13)	95.6056(9)	95.5715(11)	95.5570(11)
γ (°)	103.7254(10)	103.6370(13)	103.8057(10)	103.7060(12)	103.6592(13)
V ($Å^3$)	13512.0(3)	13510.8(4)	13171.6(2)	13473.3(4)	13444.1(4)
μ (mm^{-1})	16.154	16.200	16.658	16.334	16.414
reflns collected	165635	169180	174188	156825	185801
unique reflns (R_{int})	63917 (0.064)	65068 (0.121)	63533 (0.050)	62930 (0.062)	62891 (0.088)
Observed reflns [$I > 2\sigma(I)$]	37765	28615	40822	37410	33882
Params. / restr.	2472 / 25	1432 / 0	2524 / 20	2614 / 6	2255 / 32
R (F)[a] [$I > 2\sigma(I)$]	0.080	0.100	0.073	0.068	0.078
w$R(F^2)$[b] [all data]	0.218	0.314	0.187	0.194	0.224
GoF	1.029	1.008	1.021	1.059	1.037
	1_{Ge}-Ho	**1_{Ge}-Er**	**1_{Ge}-Tm**	**1_{Ge}-Yb**	**1_{Ge}-Lu**
empirical formula	$C_{20}H_{50}Br_2GeHoK_5N_2O_{57}W_{11}$	$C_{20}H_{50}Br_2ErGeK_5N_2O_{57}W_{11}$	$C_{20}H_{50}Br_2GeK_5N_2O_{57}TmW_{11}$	$C_{20}H_{50}Br_2GeK_5N_2O_{57}W_{11}Yb$	$C_{20}H_{50}Br_2GeK_5LuN_2O_{57}W_{11}$
fw ($g \cdot mol^{-1}$)	3845.81	3848.14	3849.81	3853.92	3855.85
crystal system	triclinic	triclinic	triclinic	triclinic	triclinic
space group (number)	$P\bar{1}$ (2)	$P\bar{1}$ (2)	$P\bar{1}$ (2)	$P\bar{1}$ (2)	$P\bar{1}$ (2)
a (Å)	21.7739(4)	21.8082(3)	21.7523(3)	21.7261(6)	21.7984(3)
b (Å)	24.6949(4)	24.7252(4)	24.7225(4)	24.6855(8)	24.7149(5)
c (Å)	28.2838(4)	28.3218(4)	28.3613(4)	28.2706(9)	28.4125(4)
α (°)	114.0507(16)	114.1567(13)	113.6550(14)	113.912(3)	113.4402(14)
β (°)	95.5598(14)	95.6577(11)	95.5392(12)	95.546(3)	95.5533(13)
γ (°)	103.6514(15)	103.6855(12)	103.6436(14)	103.741(3)	103.6491(13)
V ($Å^3$)	13172.3(4)	13205.5(3)	13259.3(4)	13142.5(8)	13331.6(4)
μ (mm^{-1})	16.803	16.815	16.801	17.005	16.822
reflns collected	152555	162973	186759	90530	158544
unique reflns (R_{int})	53135 (0.086)	53837 (0.106)	63149 (0.059)	51946 (0.109)	52368 (0.053)
Observed reflns [$I > 2\sigma(I)$]	28685	32353	39999	22864	37169
Params. / restr.	2221 / 49	2256 / 66	2578 / 36	1508 / 20	2118 / 12
R (F)[a] [$I > 2\sigma(I)$]	0.072	0.070	0.061	0.099	0.056
w$R(F^2)$[b] [all data]	0.216	0.198	0.175	0.296	0.157
GoF	1.034	1.061	1.050	1.023	1.024

[a] $R(F) = \sum||F_o - F_c||/\sum|F_o|$. [b] $wR(F^2) = \{\sum[w(F_o^2 - F_c^2)^2]/\sum[w(F_o^2)^2]\}^{1/2}$.

Table S3. Lanthanide-Oxygen bond lengths (Å) and Ln···Ln distances (Å) in compounds **1_{Ge}-Ln**.

		1_{Ge}-Sm	**1_{Ge}-Eu**	**1_{Ge}-Gd**	**1_{Ge}-Tb**	**1_{Ge}-Dy**
Ln1A-O1LA	**O_a**	2.420(14)	2.454(17)	2.391(13)	2.490(13)	2.363(15)
Ln1A-O4LA		2.493(15)	2.54(2)	2.481(14)	2.392(12)	2.460(16)
Ln1A-O2LA	**O_p**	2.387(14)	2.333(17)	2.363(12)	2.306(12)	2.325(14)
Ln1A-O3LA		2.344(13)	2.306(15)	2.322(13)	2.334(11)	2.308(14)
Ln1A-O13A	**O_{POM}**	2.396(14)	2.371(19)	2.402(12)	2.409(11)	2.352(15)
Ln1A-O15A		2.429(13)	2.398(16)	2.394(12)	2.362(12)	2.387(13)
Ln1A-O16A		2.373(15)	2.360(19)	2.349(13)	2.337(11)	2.354(18)
Ln1A-O17A		2.368(13)	2.347(16)	2.355(14)	2.360(11)	2.320(13)
Ln1A-$O_{central}$		3.069	3.047	3.057	3.063	3.087
Ln1B-O1LB	**O_a**	2.530(13)	2.377(16)	2.389(13)	2.451(14)	2.385(15)
Ln1B-O4LB		2.443(13)	2.460(19)	2.503(14)	2.372(12)	2.496(15)
Ln1B-O2LB	**O_p**	2.336(13)	2.391(19)	2.351(12)	2.312(12)	2.337(14)
Ln1B-O3LB		2.393(13)	2.339(17)	2.306(12)	2.343(12)	2.284(13)
Ln1B-O13B	**O_{POM}**	2.442(13)	2.377(17)	2.386(12)	2.400(11)	2.372(15)
Ln1B-O15B		2.411(13)	2.416(17)	2.419(12)	2.366(11)	2.422(16)
Ln1B-O16B		2.393(15)	2.375(18)	2.371(13)	2.355(11)	2.321(14)
Ln1B-O17B		2.364(14)	2.347(17)	2.367(11)	2.349(13)	2.319(14)
Ln1B-$O_{central}$		3.070	3.066	3.076	3.081	3.049
Ln1C-O1LC	**O_a**	2.546(16)	2.541(18)	2.500(13)	2.496(11)	2.378(14)
Ln1C-O4LC		2.428(14)	2.462(16)	2.405(12)	2.411(12)	2.510(13)
Ln1C-O2LC	**O_p**	2.327(14)	2.331(15)	2.311(12)	2.318(11)	2.347(13)
Ln1C-O3LC		2.367(14)	2.376(18)	2.364(12)	2.357(12)	2.303(15)
Ln1C-O13C	**O_{POM}**	2.402(15)	2.409(14)	2.427(12)	2.407(10)	2.357(14)
Ln1C-O15C		2.450(13)	2.436(16)	2.383(13)	2.382(10)	2.396(14)
Ln1C-O16C		2.381(13)	2.374(18)	2.348(12)	2.352(11)	2.308(13)
Ln1C-O17C		2.373(13)	2.361(18)	2.352(12)	2.341(11)	2.324(14)
Ln1C-$O_{central}$		3.051	3.101	3.051	3.083	3.082
O_a (average)		2.477	2.472	2.445	2.435	2.432
O_p (average)		2.359	2.346	2.336	2.328	2.317
O_{POM} (average)		2.399	2.381	2.379	2.368	2.353
LnA···LnB		8.200	8.120	8.122	8.112	8.126
LnB···LnC		8.289	8.209	8.239	8.202	8.266
LnC···LnA		8.109	8.284	8.115	8.287	8.266

Abbreviations: O_a: O atoms from the aldehyde group of the H_2L ligand; O_p: O atoms from the phenoxy group of the H_2L ligand; O_{POM}: O atoms delimiting the vacant site of the lacunary Keggin-type POM.

Table S3 (*continuation*). Lanthanide-Oxygen bond lengths (Å) and Ln···Ln distances (Å) in compounds **1_{Ge}-Ln**.

		1_{Ge}-Ho	**1_{Ge}-Er**	**1_{Ge}-Tm**	**1_{Ge}-Yb**	**1_{Ge}-Lu**
Ln1A-O1LA	**O_a**	2.44(2)	2.415(13)	2.455(11)	2.42(3)	2.428(12)
Ln1A-O4LA		2.346(16)	2.359(12)	2.356(11)	2.30(2)	2.334(10)
Ln1A-O2LA	**O_p**	2.287(15)	2.247(13)	2.258(11)	2.24(2)	2.228(10)
Ln1A-O3LA		2.299(15)	2.310(12)	2.312(10)	2.29(2)	2.288(10)
Ln1A-O13A	**O_{POM}**	2.357(16)	2.367(11)	2.369(10)	2.38 (2)	2.336(11)
Ln1A-O15A		2.340(16)	2.356(12)	2.350(10)	2.29(2)	2.305(10)
Ln1A-O16A		2.306(17)	2.315(12)	2.309(10)	2.284(19)	2.293(10)
Ln1A-O17A		2.297(16)	2.287(13)	2.319(10)	2.28(2)	2.286(10)
Ln1A-$O_{central}$		3.075	3.081	3.079	3.074	3.065
Ln1B-O1LB	**O_a**	2.482(16)	2.363(12)	2.351(10)	2.50(2)	2.416(12)
Ln1B-O4LB		2.382(15)	2.452(13)	2.438(11)	2.33(2)	2.322(10)
Ln1B-O2LB	**O_p**	2.304(16)	2.306(12)	2.298(10)	2.270(18)	2.255(11)
Ln1B-O3LB		2.316(15)	2.258(12)	2.236(11)	2.28(2)	2.294(12)
Ln1B-O13B	**O_{POM}**	2.378(16)	2.354(12)	2.328(10)	2.36(2)	2.345(10)
Ln1B-O15B		2.335(17)	2.377(14)	2.362(10)	2.333(19)	2.305(10)
Ln1B-O16B		2.309(16)	2.315(13)	2.298(10)	2.28(2)	2.290(11)
Ln1B-O17B		2.333(17)	2.316(12)	2.313(10)	2.29(2)	2.290(12)
Ln1B-$O_{central}$		3.080	3.103	3.056	3.097	3.093
Ln1C-O1LC	**O_a**	2.454(18)	2.454(14)	2.405(12)	2.29(2)	2.329(11)
Ln1C-O4LC		2.385(17)	2.355(12)	2.358(10)	2.46(2)	2.472(11)
Ln1C-O2LC	**O_p**	2.262(16)	2.247(11)	2.274(10)	2.298(19)	2.299(9)
Ln1C-O3LC		2.304(15)	2.307(12)	2.313(10)	2.28(2)	2.243(10)
Ln1C-O13C	**O_{POM}**	2.392(17)	2.386(13)	2.360(11)	2.37(2)	2.318(11)
Ln1C-O15C		2.336(16)	2.317(14)	2.304(10)	2.393(19)	2.353(10)
Ln1C-O16C		2.326(15)	2.281(11)	2.200(10)	2.311(19)	2.291(11)
Ln1C-O17C		2.328(16)	2.303(12)	2.306(12)	2.30(2)	2.294(10)
Ln1C-$O_{central}$		3.046	3.046	3.061	3.090	3.084
O_a (average)		2.415	2.400	2.394	2.383	2.384
O_p (average)		2.295	2.279	2.282	2.276	2.268
O_{POM} (average)		2.336	2.331	2.318	2.323	2.309
LnA···LnB		8.122	8.116	8.249	8.112	8.133
LnB···LnC		8.251	8.254	8.124	8.233	8.201
LnC···LnA		8.103	8.099	8.177	8.125	8.266

Abbreviations: O_a: O atoms from the aldehyde group of the H_2L ligand; O_p: O atoms from the phenoxy group of the H_2L ligand; O_{POM}: O atoms delimiting the vacant site of the lacunary Keggin-type POM.

Table S4. Intramolecular centroid···centroid (Cg···Cg) distances (Å) (top) and dihedral angles (°) (bottom) between aromatic rings of the H_2L ligand in compounds **1_{Ge}-Ln**.

	1_{Ge}-Sm	**1_{Ge}-Eu**	**1_{Ge}-Gd**	**1_{Ge}-Tb**	**1_{Ge}-Dy**	**1_{Ge}-Ho**	**1_{Ge}-Er**	**1_{Ge}-Tm**	**1_{Ge}-Yb**	**1_{Ge}-Lu**
LnA	6.436	6.530	6.498	6.490	6.378	6.424	6.390	6.324	6.407	6.393
LnB	6.409	6.379	6.445	6.361	6.478	6.359	6.352	6.409	6.442	6.307
LnC	6.542	6.392	6.518	6.362	6.355	6.473	6.482	6.344	6.363	6.297
	1_{Ge}-Sm	**1_{Ge}-Eu**	**1_{Ge}-Gd**	**1_{Ge}-Tb**	**1_{Ge}-Dy**	**1_{Ge}-Ho**	**1_{Ge}-Er**	**1_{Ge}-Tm**	**1_{Ge}-Yb**	**1_{Ge}-Lu**
LnA	85.816	87.471	88.472	89.691	86.241	85.158	85.386	85.353	89.463	88.908
LnB	83.415	86.864	89.913	85.390	90.189	83.447	88.814	89.090	88.142	88.262
LnC	87.608	84.181	89.882	82.242	83.366	89.413	87.397	84.879	85.967	89.896

Table S5. Geometrical parameters (Å, °) of intermolecular π–π interactions in **1_{Ge}-Ln**.

Centroids	Cg···Cg	ANG	Slippage	Centroids	Cg···Cg	ANG	Slippage
1_{Ge}-Sm				**1_{Ge}-Ho**			
Cg1···Cg5^{i}	3.578(15)	4	0.625	Cg1···Cg4^{xii}	3.597(19)	6	0.962
Cg2···Cg4^{ii}	3.586(15)	7	1.008	Cg2···Cg5^{xiii}	3.587(17)	4	0.642
Cg3···Cg6^{iii}	3.609(13)	6	1.198	Cg3···Cg6^{xiv}	3.584(15)	7	1.206
Cg4···Cg2^{iv}	3.585(15)	7	0.588	Cg4···Cg1^{xii}	3.598(19)	6	0.569
Cg5···Cg1^{i}	3.579(15)	4	0.864	Cg5···Cg2^{xiii}	3.586(17)	4	0.851
Cg6···Cg3^{v}	3.608(13)	6	0.827	Cg6···Cg3^{xiv}	3.585(15)	7	0.831
1_{Ge}-Eu				**1_{Ge}-Er**			
Cg1···Cg5^{v}	3.613(16)	7	0.825	Cg1···Cg3^{xv}	3.571(13)	6	0.966
Cg2···Cg3^{vi}	3.623(17)	5	0.903	Cg2···Cg5^{xvi}	3.599(13)	5	0.652
Cg3···Cg2^{vi}	3.624(17)	5	0.597	Cg3···Cg1^{xvi}	3.569(13)	6	0.578
Cg4···Cg6^{ii}	3.596(17)	8	0.977	Cg4···Cg6^{xvii}	3.593(11)	6	1.151
Cg5···Cg1^{iii}	3.612(16)	7	1.247	Cg5···Cg2^{xvi}	3.600(13)	5	0.925
Cg6···Cg4^{iv}	3.596(17)	8	0.478	Cg6···Cg4^{xvii}	3.592(11)	6	0.827
1_{Ge}-Gd				**1_{Ge}-Tm**			
Cg1···Cg5^{vii}	3.559(13)	3	0.626	Cg1···Cg3^{iii}	3.613(10)	6	1.231
Cg2···Cg3^{iv}	3.583(14)	4	0.860	Cg2···Cg5^{vii}	3.596(11)	6	0.630
Cg3···Cg2^{ii}	3.585(14)	4	0.587	Cg3···Cg1^{v}	3.614(10)	6	0.878
Cg4···Cg6^{viii}	3.577(12)	6	1.124	Cg4···Cg6^{xviii}	3.596(11)	5	0.915
Cg5···Cg1^{vii}	3.560(13)	3	0.818	Cg5···Cg2^{vii}	3.596(11)	6	1.017
Cg6···Cg4^{viii}	3.577(12)	6	0.802	Cg6···Cg4^{xix}	3.596(11)	5	0.610
1_{Ge}-Tb				**1_{Ge}-Yb**			
Cg1···Cg4^{ix}	3.591(12)	4	0.853	Cg1···Cg4^{ii}	3.56(3)	6	0.889
Cg2···Cg5^{iii}	3.608(11)	7	0.863	Cg2···Cg5^{iv}	3.55(3)	6	0.551
Cg3···Cg6^{iv}	3.584(12)	9	1.080	Cg3···Cg6^{iii}	3.59(3)	6	0.906
Cg4···Cg1^{ix}	3.591(12)	4	0.614	Cg4···Cg1^{ii}	3.56(3)	6	0.889
Cg5···Cg2^{v}	3.608(11)	7	1.239	Cg5···Cg2^{iv}	3.55(3)	6	0.551
Cg6···Cg3^{ii}	3.582(12)	9	0.562	Cg6···Cg3^{iii}	3.59(3)	6	0.906
1_{Ge}-Dy				**1_{Ge}-Lu**			
Cg1···Cg4^{x}	3.598(15)	4	0.663	Cg1···Cg4^{xx}	3.616(11)	6	0.964
Cg2···Cg5^{ix}	3.592(15)	7	1.033	Cg2···Cg6^{v}	3.623(10)	8	0.865
Cg3···Cg6^{xi}	3.605(13)	6	0.824	Cg3···Cg5^{ii}	3.608(12)	7	1.095
Cg4···Cg1^{x}	3.600(15)	4	0.887	Cg4···Cg1^{xx}	3.615(11)	6	0.623
Cg5···Cg2^{vii}	3.593(15)	7	0.585	Cg5···Cg3^{iv}	3.608(12)	7	0.689
Cg6···Cg3^{xi}	3.606(13)	6	1.174	Cg6···Cg2^{iii}	3.624(10)	8	1.277

Cgi = Centroid of the aromatic ring defined by the following atoms: i = 1: C2A, C3A, C4A, C5A, C6A, C7A; i = 2: C12A, C13A, C14A, C15A, C16A, C17A; i = 3: C2B, C3B, C4B, C5B, C6B, C7B; i = 4: C12B, C13B, C14B, C15B, C16B, C17B; i = 5: C2C, C3C, C4C, C5C, C6C, C7C; i = 6: C12C, C13C, C14C, C15C, C16C, C17C. Cg···Cg = distance between centroids; ANG = dihedral angle between planes containing both rings; Slippage = distance between one centroid and its perpendicular projection to the plane containing the second ring. Symmetry codes: (i) 1-x, -y, -z; (ii) x, -1+y, z; (iii) -1+x, y, z; (iv) x, 1+y, z; (v) 1+x, y, z; (vi) 1-x, -y, 1-z; (vii) -x, 1-y, 2-z; (viii) x, y, z; (ix) -x, 2-y, 1-z; (x) -x, 1-y, 1-z; (xi) 1-x, 2-y, 2-z; (xii) 2-x, 1-y, 2-z; (xiii) 2-x, -y, 2-z; (xiv) 1-x, -y, 2-z; (xv) -x, -y, 2-z; (xvi) -x, -y, 1-z; (xvii) 1-x, 1-y, 2-z; (xviii) x, 1-y, -1+z; (xix) x, 1+y, 1+z; (xx) 2-x, -y, -z.

Table S6. Br···Br distances (Å) in compounds **1_{Ge}-Ln**.

Br···Br	**1_{Ge}-Sm**[a]	**1_{Ge}-Eu**[b]	**1_{Ge}-Gd**[c]	**1_{Ge}-Tb**[d]	**1_{Ge}-Dy**[e]
BrA-BrB	3.718(6)	3.917(5)	3.751(5)	3.935(5)	3.899(6)
BrB-BrC	3.997(7)	3.698(7)	3.871(6)	3.711(5)	3.935(4)
BrC-BrA	3.938(5)	3.961(8)	3.999(4)	3.952(6)	3.715(6)
	1_{Ge}-Ho[f]	**1_{Ge}-Er**[g]	**1_{Ge}-Tm**[h]	**1_{Ge}-Yb**[j]	**1_{Ge}-Lu**[k]
BrA-BrB	3.701(7)	3.672(4)	3.899(3)	3.925(7)	3.880(4)
BrB-BrC	3.866(8)	3.867(6)	3.920(4)	3.848(6)	3.715(3)
BrC-BrA	3.973(5)	3.964(5)	3.723(3)	3.699(6)	3.922(5)

Symmetry codes: [a] Br1A···Br2B^{i}: -x, -y, -z; Br2C···Br2B^{ii}: 1-x, 1-y, -z; Br1A···Br2C^{iii}: 1+x, 1+y, z; [b] Br1A···Br1B^{iii}; Br2C···Br1B^{iv}: -x, -y, 1-z; Br1A···Br2C^{v}: 1-x, 1-y, 1-z; [c] Br2A···Br1B^{vi}: -x, 1-y, 2-z; Br1B···Br2C^{vii}: -x, -y, 2-z; Br2A···Br2C^{viii}: x, 1+y, z; [d] Br2A···Br2B^{ix}: -1+x, -1+y, z; Br2C···Br2B^{x}: -1+x, -1+y, -1+z; Br2A···Br2C^{xi}: x, y, 1+z; [e] Br1A···Br1B^{ix}; Br1C···Br1B^{xi}; Br1A···Br1C^{x}; [f] Br2A···Br2B^{xii}: 1+x, 1+y, 1+z; Br2C···Br2B^{xi}; Br2A···Br2C^{ii}; [g] Br2A···Br1B^{xiii}: 1-x, 2-y, 1-z; Br2C···Br1B^{xiv}: -x, 1-y, 1-z; Br2A···Br2C^{xi}; [h] Br2A···Br1B^{iv}; Br2C···Br1B^{xv}: 1-x, 1-y, 2-z; Br2A···Br2C^{x}; [j] Br2A···Br2B^{viii}; Br1C···Br2B^{v}; Br2A···Br1C^{xiii}; [k] Br2A···Br2B; Br1C···Br2B^{xv}; Br2A···Br1C^{xv}.

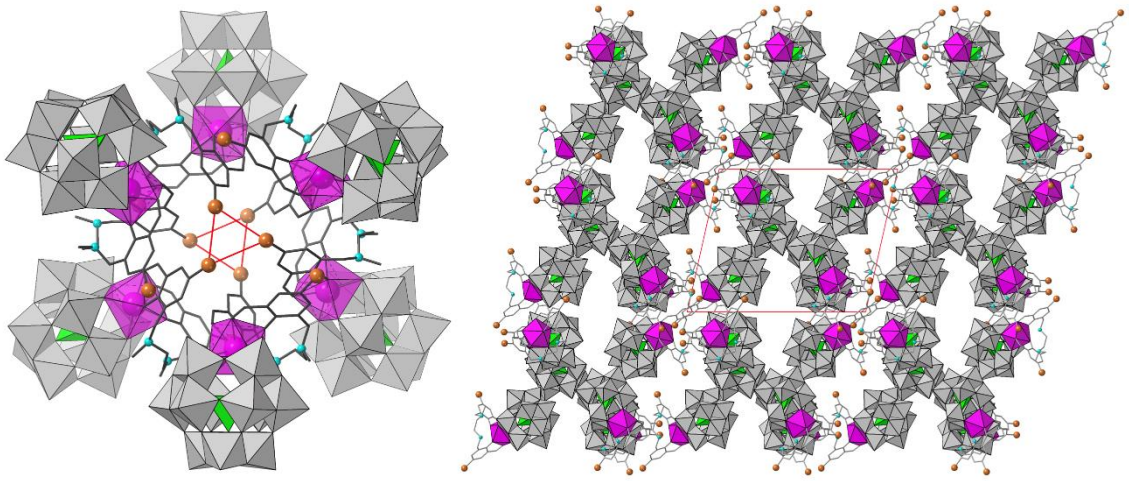

Figure S7. Left: Hexameric chairlike supramolecular assemblies in **1_{Ge}-Ln**. Intermolecular Br···Br contacts are represented as red lines. Right: View of the crystal packing along the [010] direction for **1_{Ge}-Ln**. Colour code: WO_6, grey; GeO_4, green; LnO_8, pink; C, black; N, blue; Br, orange.

Continuous Shape Measurements

Table S7. Continuous Shape Measurements (CSM) for the eight coordinated lanthanide atoms in compounds **1_{Ge}-Ln**.[a]

	Atom	Geometry	1_{Ge}-Sm	1_{Ge}-Eu	1_{Ge}-Gd	1_{Ge}-Tb	1_{Ge}-Dy	1_{Ge}-Ho	1_{Ge}-Er	1_{Ge}-Tm	1_{Ge}-Yb	1_{Ge}-Lu
1_{Ge}-Ln	Ln1A	SAPR-8	0.970	1.039	0.978	0.970	0.977	0.922	0.903	0.949	0.943	0.986
		BTPR-8	0.654	0.617	0.614	0.642	0.572	0.633	0.659	0.630	0.687	0.625
	Ln1B	SAPR-8	1.038	0.970	1.011	0.952	0.981	1.019	1.012	0.957	1.002	0.937
		BTPR-8	0.631	0.594	0.597	0.608	0.661	0.653	0.627	0.628	0.707	0.615
	Ln1C	SAPR-8	1.006	1.061	0.974	0.965	1.051	0.889	0.902	0.852	1.002	0.987
		BTPR-8	0.622	0.556	0.664	0.637	0.643	0.661	0.691	0.673	0.667	0.658
1_{Si}-Ln	Ln1A	SAPR-8	0.941	1.007	0.950	0.873	0.947	0.995	0.943	0.914	0.903	0.900
		BTPR-8	0.766	0.785	0.796	0.869	0.785	0.725	0.722	0.841	0.799	0.819
	Ln1B	SAPR-8	1.059	1.015	1.066	0.974	0.943	0.901	0.997	0.867	0.907	0.896
		BTPR-8	0.785	0.696	0.710	0.671	0.812	0.865	0.685	0.781	0.828	0.763
	Ln1C	SAPR-8	1.052	1.034	1.044	0.917	0.965	0.904	0.983	1.041	0.911	0.889
		BTPR-8	0.857	0.837	0.766	0.809	0.762	0.776	0.720	0.776	0.823	0.804

[a] *Abbreviations*. **SAPR:** square antiprism (D_{4d}) and **BTPR:** biaugmented trigonal prism (C_{2v}).

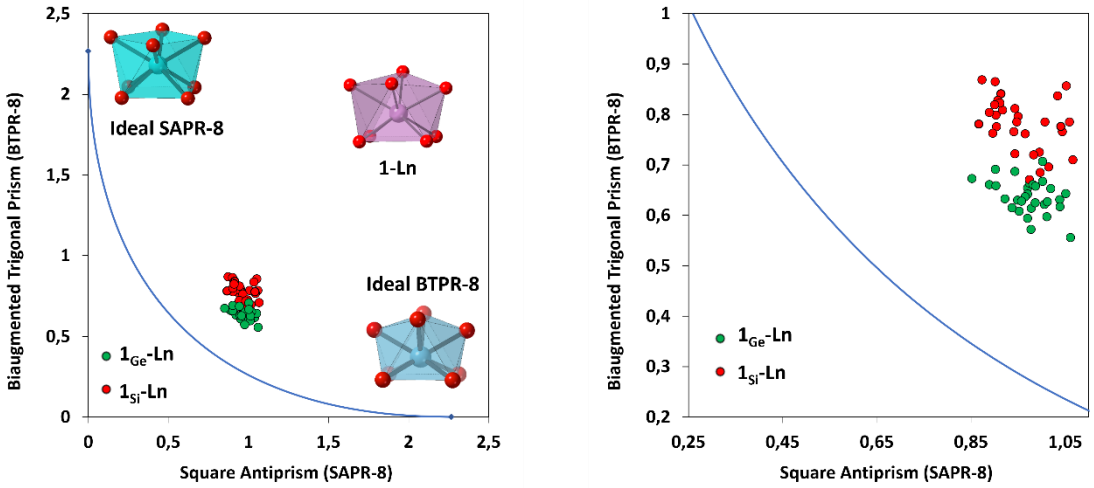

Figure S8. Biaugmented trigonal prism (BTPR) vs. square antiprism (SAPR) shape maps for the LnO_8 coordination polyhedra of 4f ions in **1_{Ge}-Ln** and **1_{Si}-Ln**. Solid line: minimal distortion pathway between reference shapes.

Magnetic Properties

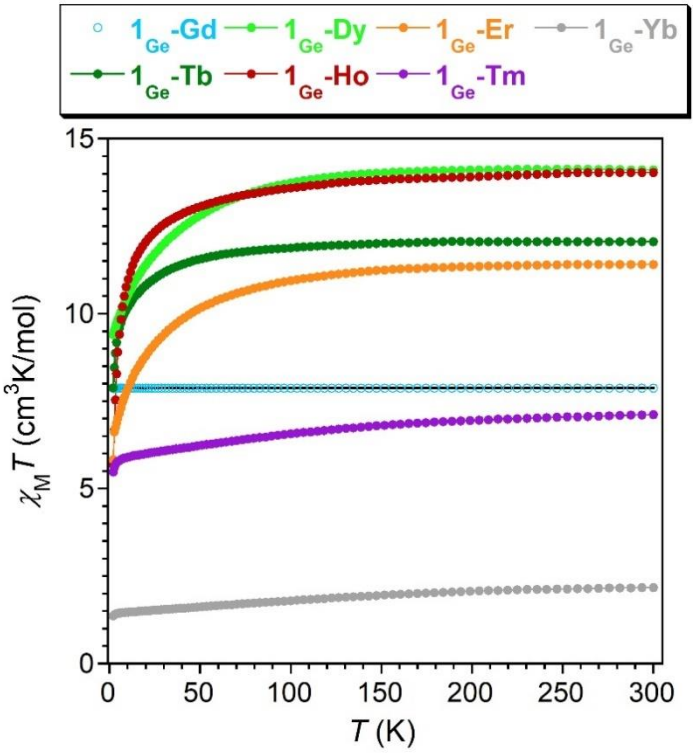

Figure S9. Temperature dependence of the $\chi_M T$ product at 5000 Oe for **1_{Ge}-Yb** and at 1000 Oe for the rest of **1_{Ge}-Ln** complexes. The black line represents the fitting of **1_{Ge}-Gd** as discussed in the text. The rest of the lines are a guide for the eye.

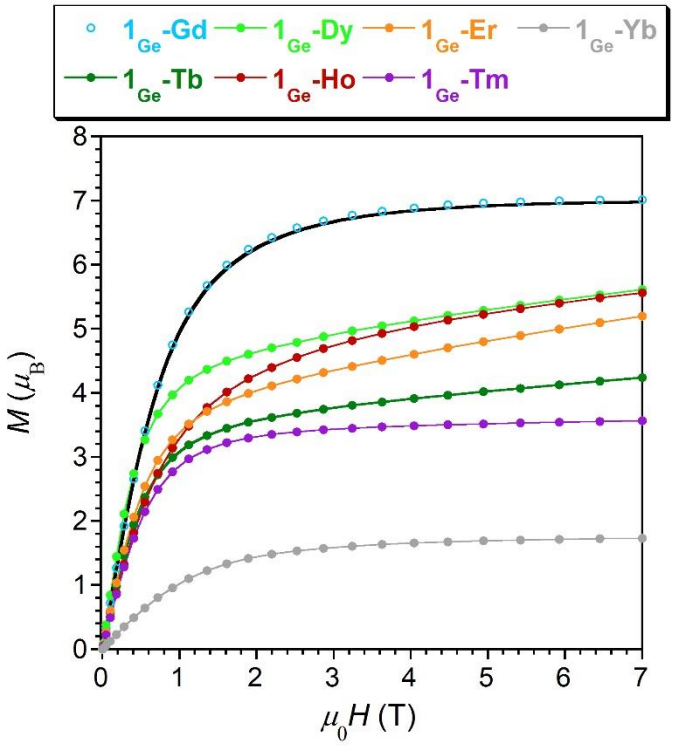

Figure S10. Field dependent magnetization plots at 2 K for complexes **1_{Ge}-Ln**. The black line represents the fitting of **1_{Ge}-Gd** as discussed in the text. The rest of the lines are a guide for the eye.

Table S8. Direct current magnetic data for **1_{Ge}-Ln**.

	Ground-state of Ln^{III} ion[a]	$\chi_M T$ (cm³K/mol)			*M* (μ_B)	
		Theor.[b] 300 K	Exp. 300 K	Exp. 2 K	Theor.[c]	Exp.2 K and 7 T
1_{Ge}-Sm	$^6H_{5/2}$, g_j = 2/7	0.09	0.35	0.022	0.71	0.15
1_{Ge}-Eu	$^7F_0$, g_j = 0	0	1.39	0.019	0	0.09
1_{Ge}-Gd	$^8S_{7/2}$, g_j = 2	7.88	7.88	7.86	7.0	7.02
1_{Ge}-Tb	$^7F_6$, g_j = 3/2	11.82	12.06	7.89	9.0	4.24
1_{Ge}-Dy	$^6H_{15/2}$, g_j = 4/3	14.17	14.12	9.40	10.0	5.61
1_{Ge}-Ho	$^5I_8$, g_j = 5/4	14.07	14.04	5.68	10.0	5.57
1_{Ge}-Er	$^4I_{15/2}$, g_j = 6/5	11.48	11.41	5.84	9.0	5.20
1_{Ge}-Tm	$^3H_6$, g_j = 7/6	7.14	7.12	5.48	7.0	3.57
1_{Ge}-Yb	$^2F_{7/2}$, g_j = 8/7	2.57	2.18	1.37	4.0	1.73

[a] $J = L - S\ (Sm, Eu); J = L + S\ (Tb - Yb);\ g_j = \frac{3}{2} + \frac{S(S+1)-L(L+1)}{2J(J+1)}$

[b] $\chi_M T = \frac{N\beta^2}{3k}\{g_j^2 J(J+1)\}$ [c] $M_s = g_j J N \mu_B$

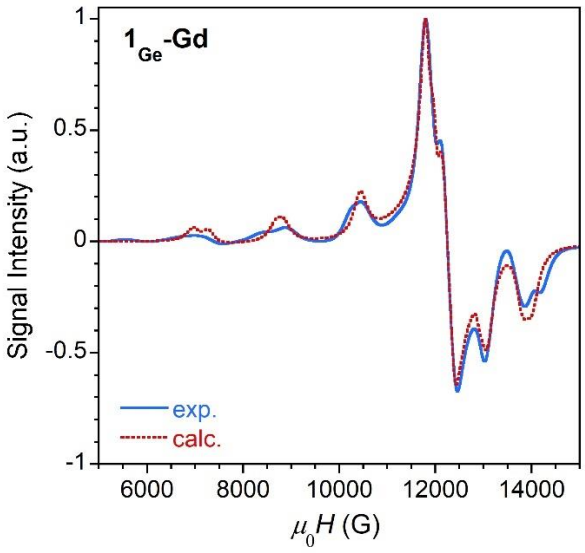

Figure S11. Q-band EPR spectra collected for **1_{Ge}-Gd** at room temperature.

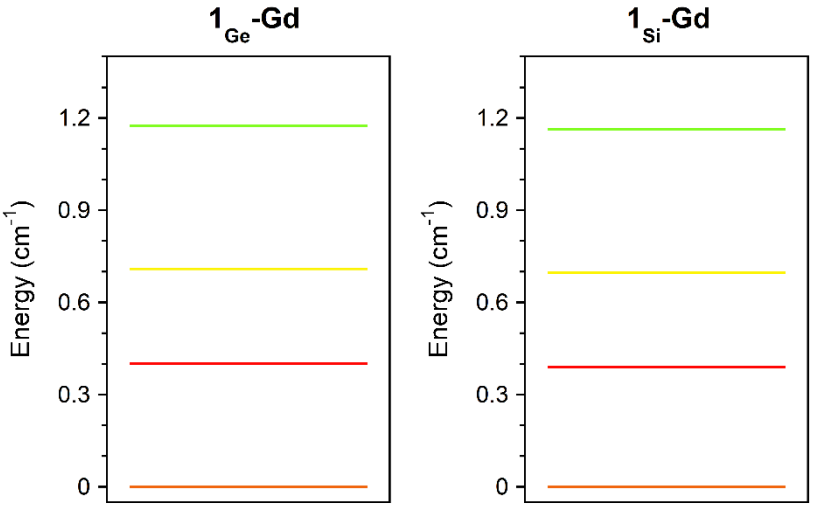

Figure S12. Energy level diagrams for **1_{Ge}-Gd** (left) and **1_{Si}-Gd** (right).

Table S9. Parameters obtained from the fitting to the Q-band EPR spectra for **1_{Ge}-Gd** and **1_{Si}-Gd**.

	1_{Ge}-Gd	**1_{Si}-Gd**
D **(cm^{-1})**	0.0831	0.0802
E **(cm^{-1})**	0.0244	0.0231
g_x	1.993	1.990
g_y	1.992	1.986
g_z	1.983	1.985

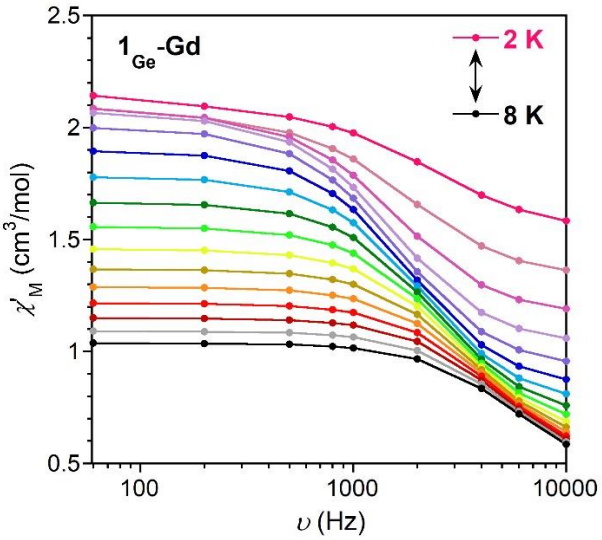

Figure S13. Frequency dependence of the in-phase component of the *ac* susceptibility at H_{dc} = 2500 Oe for **1_{Ge}-Gd**. The experimental data are denoted by circles; solid lines represent a guide to the eye.

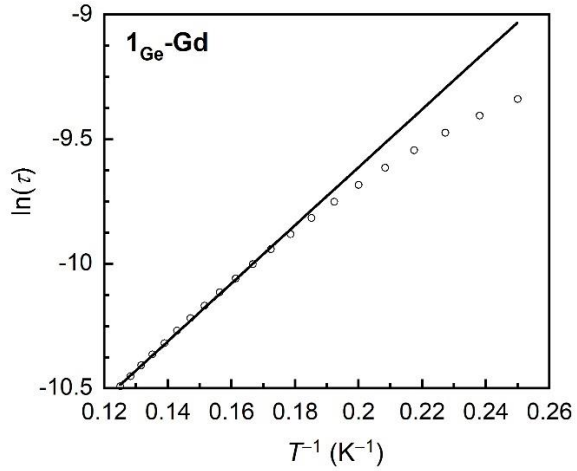

Figure S14. Arrhenius plot for the relaxation times of **1_{Ge}-Gd**. The experimental data are denoted by open circles; the solid line represents the best fit.

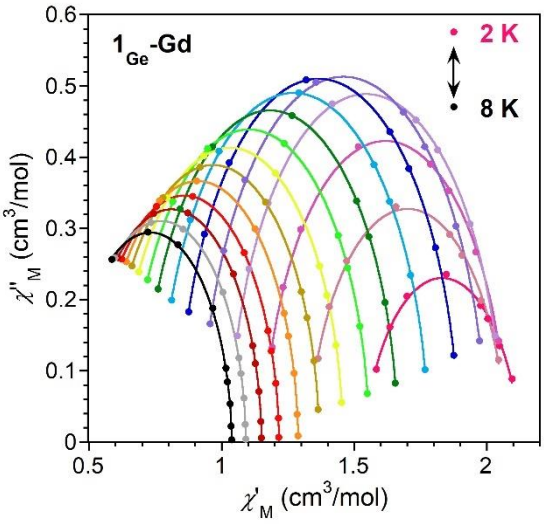

Figure S15. Cole-Cole plots for **1_{Ge}-Gd** at H_{dc} = 2500 Oe. The experimental data are denoted by circles; solid lines represent the best fit to the Debye model.

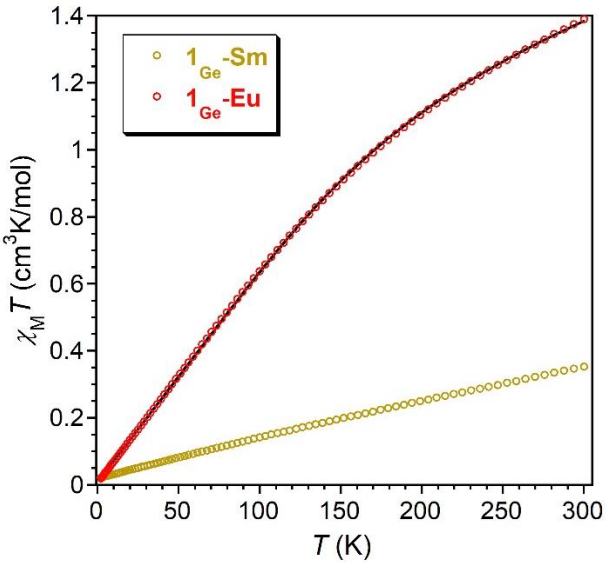

Figure S16. Temperature dependence of the $\chi_M T$ product at 1000 Oe for **1_{Ge}-Sm** and **1_{Ge}-Eu**. Black solid lines represent the best fit to the magnetic data.

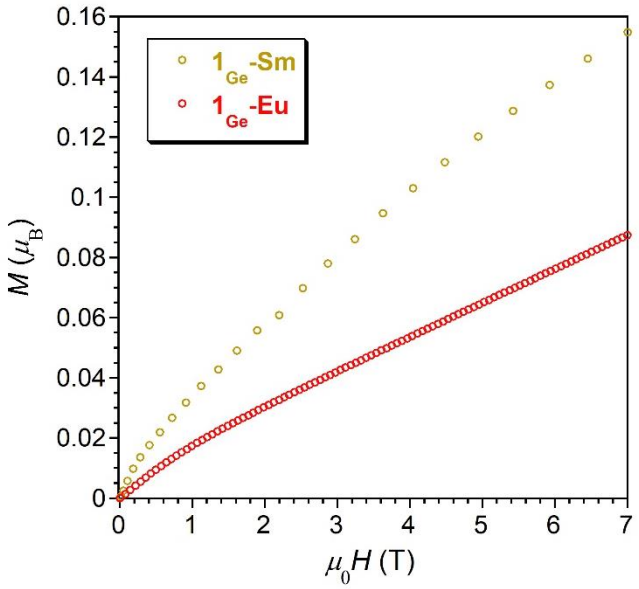

Figure S17. Field dependent magnetization plots at 2 K for **1_{Ge}-Sm** and **1_{Ge}-Eu**. Black solid lines represent the best fit to the magnetic data.

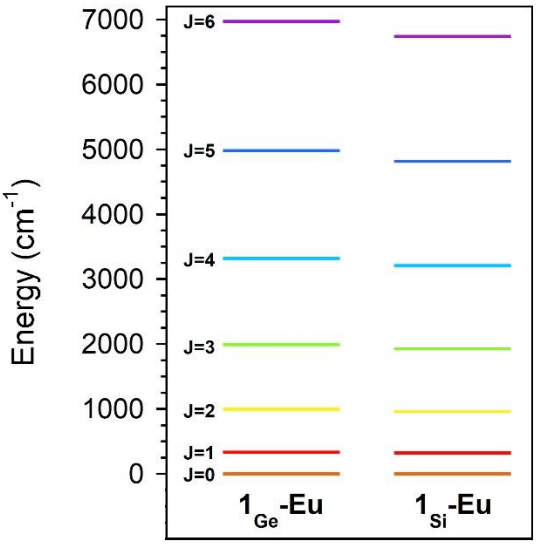

Figure S18. Energy level diagrams for **1_{Ge}-Eu** and **1_{Si}-Eu**.

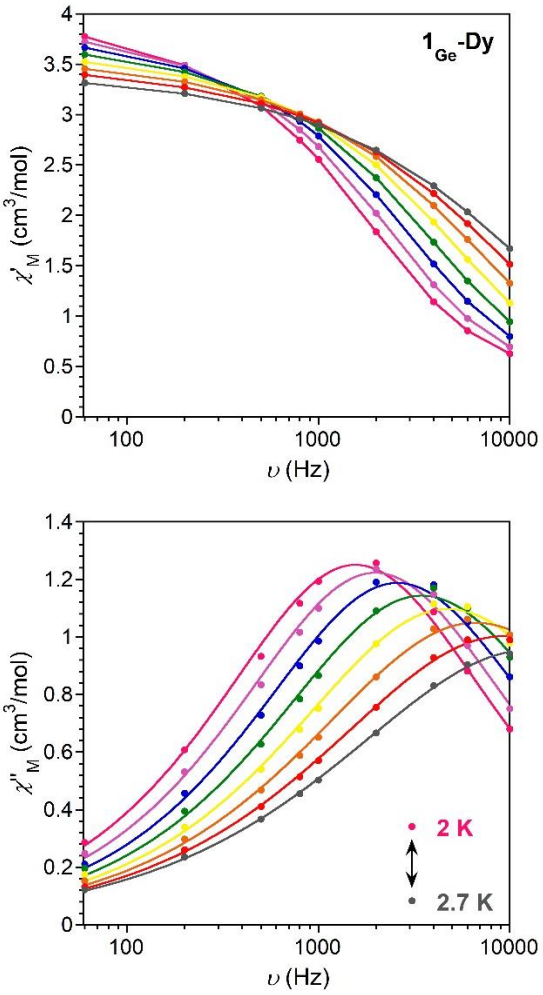

Figure S19. Frequency dependence of the in-phase (top) and out-of-phase (bottom) components of the *ac* susceptibility at H_{dc} = 1000 Oe for **1_{Ge}-Dy**. The experimental data are denoted by circles; solid lines represent a guide to the eye (top) and the best fit to the data (bottom).

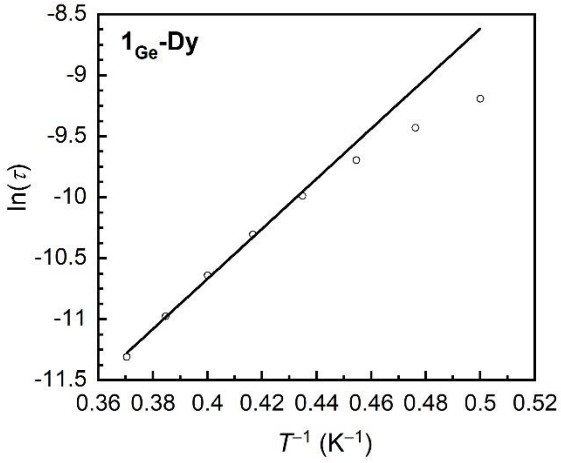

Figure S20. Arrhenius plot for the relaxation times of **1$_{Ge}$-Dy**. The experimental data are denoted by open circles; the solid line represents the best fit.

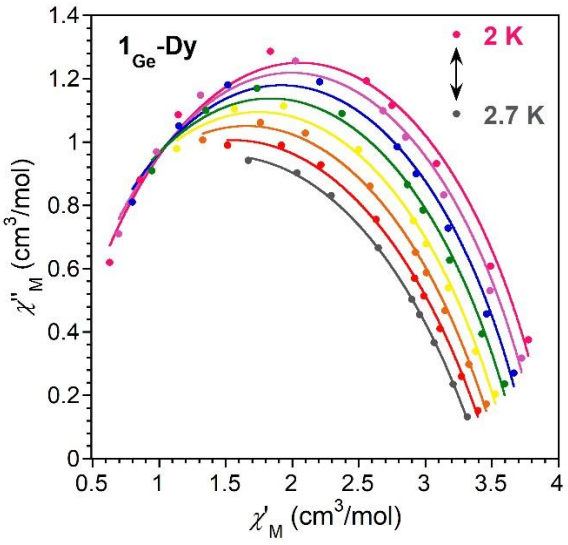

Figure S21. Cole-Cole plots for **1$_{Ge}$-Dy** at H_{dc} = 1000 Oe. The experimental data are denoted by circles; solid lines represent the best fit to the Debye model.

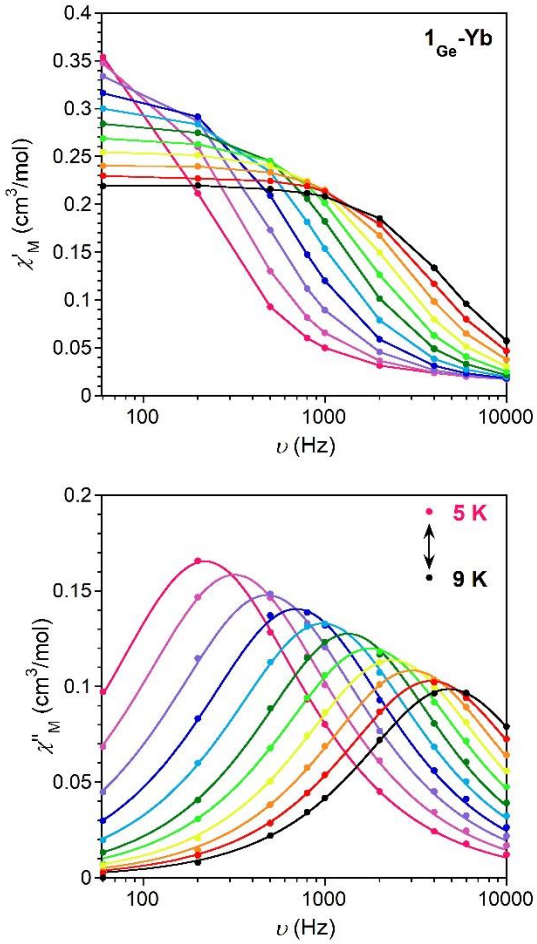

Figure S22. Frequency dependence of the in-phase (top) and out-of-phase (bottom) components of the *ac* susceptibility at H_{dc} = 1000 Oe for **1$_{Ge}$-Yb**. The experimental data are denoted by circles; solid lines represent a guide to the eye (top) and the best fit to the data (bottom).

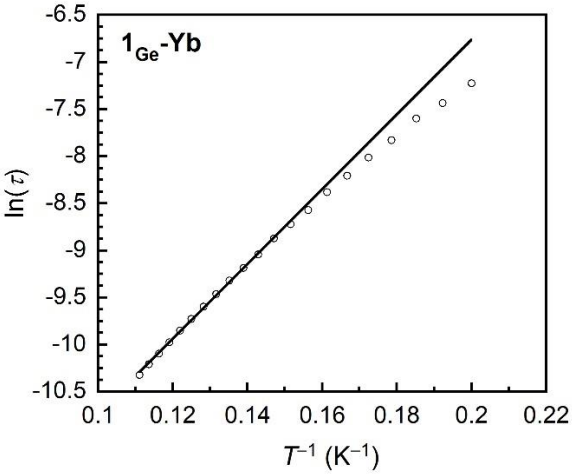

Figure S23. Arrhenius plot for the relaxation times of **1$_{Ge}$-Yb**. The experimental data are denoted by open circles; the solid line represents the best fit.

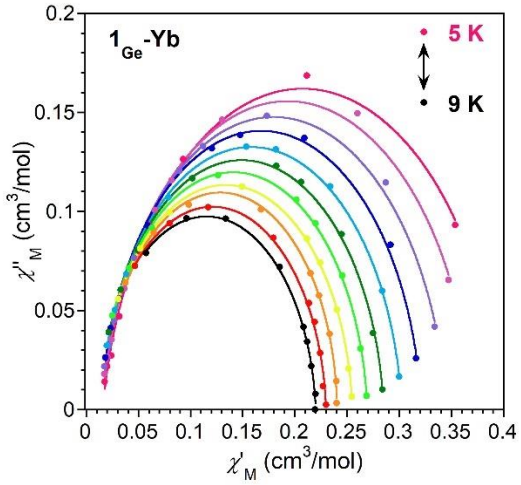

Figure S24. Cole-Cole plots for **1_{Ge}-Yb** at H_{dc} = 1000 Oe. The experimental data are denoted by circles; solid lines represent the best fit to the Debye model.

Photophysical Properties

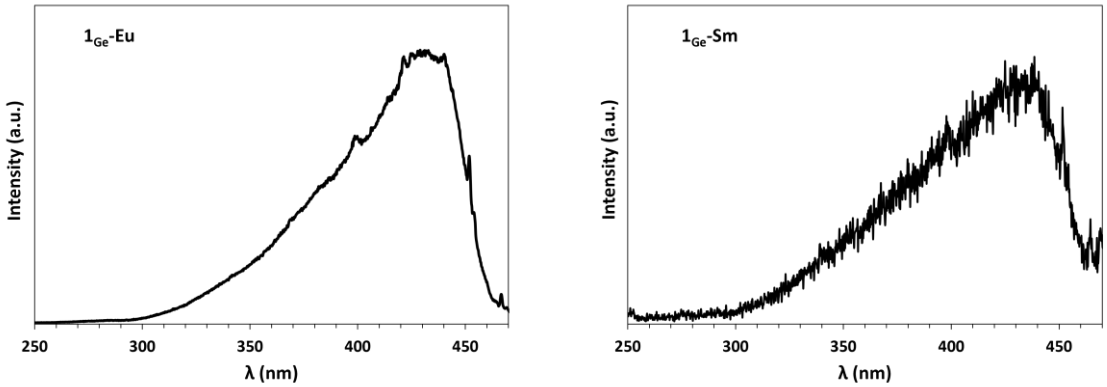

Figure S25. Low temperature (15 K) solid state excitation spectra for **1_{Ge}-Eu** (left) and **1_{Ge}-Sm** (right) recorded for their most intense emission bands (599 and 614 nm, respectively).

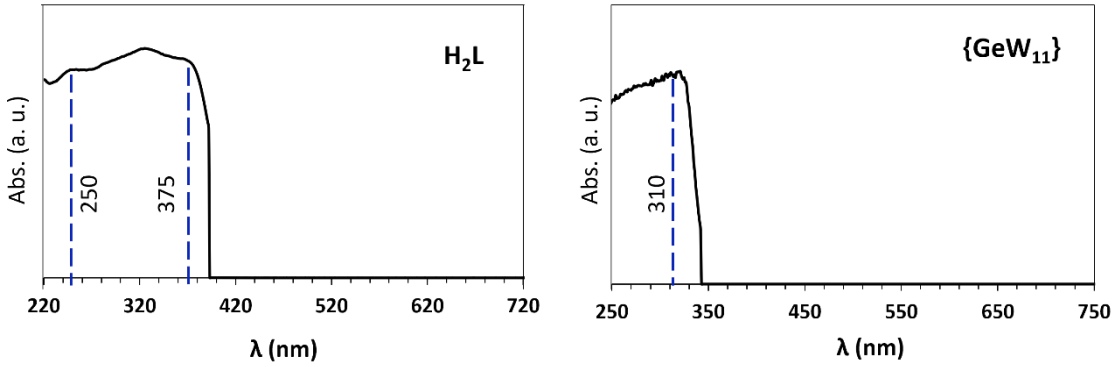

Figure S26. UV-Vis diffuse reflectance absorption spectra of H_2L ligand (left) and $K_8[\alpha\text{-}GeW_{11}O_{39}]\cdot 13H_2O$ POM precursor (right) at room temperature.

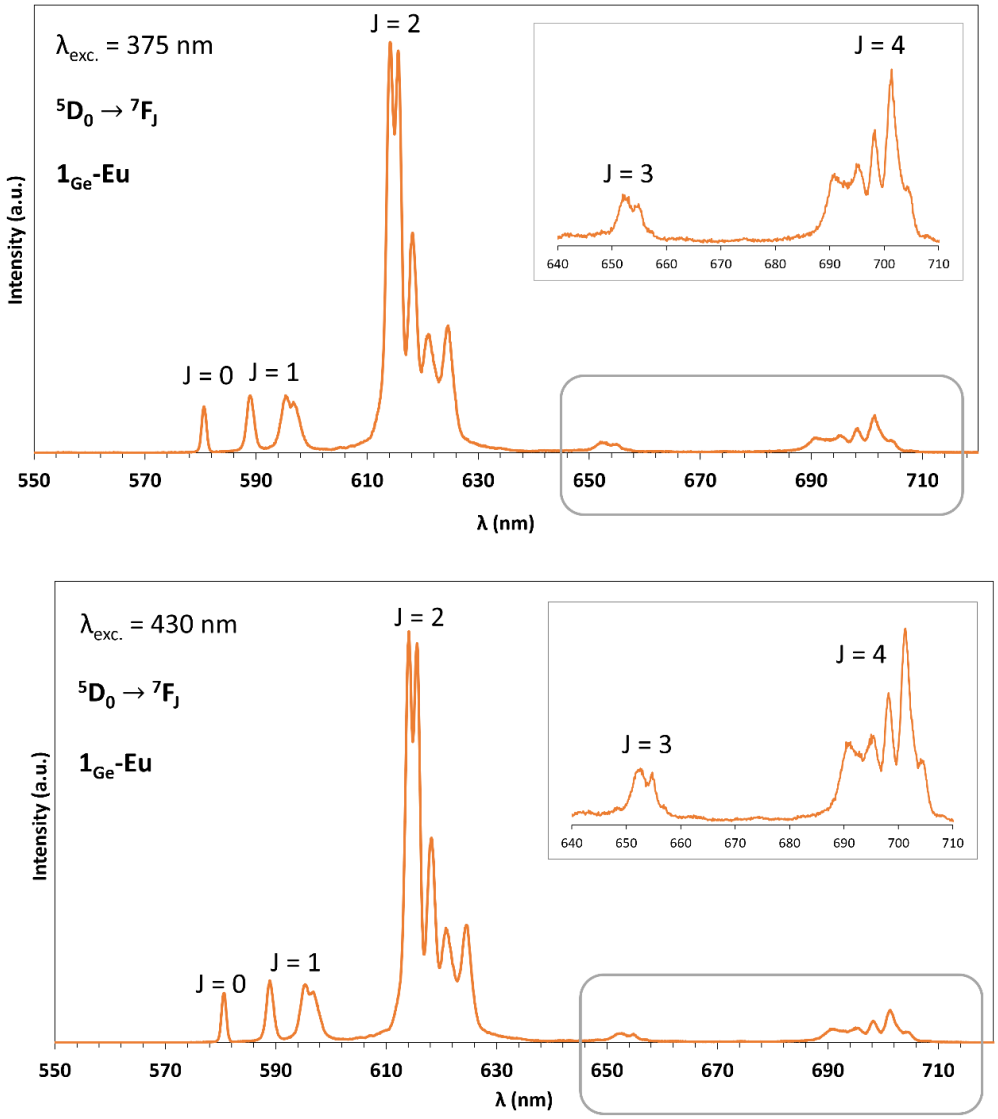

Figure S27. Solid state photoluminescence spectrum of **1_{Ge}-Eu** recorded at 15 K upon excitation at 375 nm (top) and 430 nm (bottom). Inset: detailed view of weak transition bands.

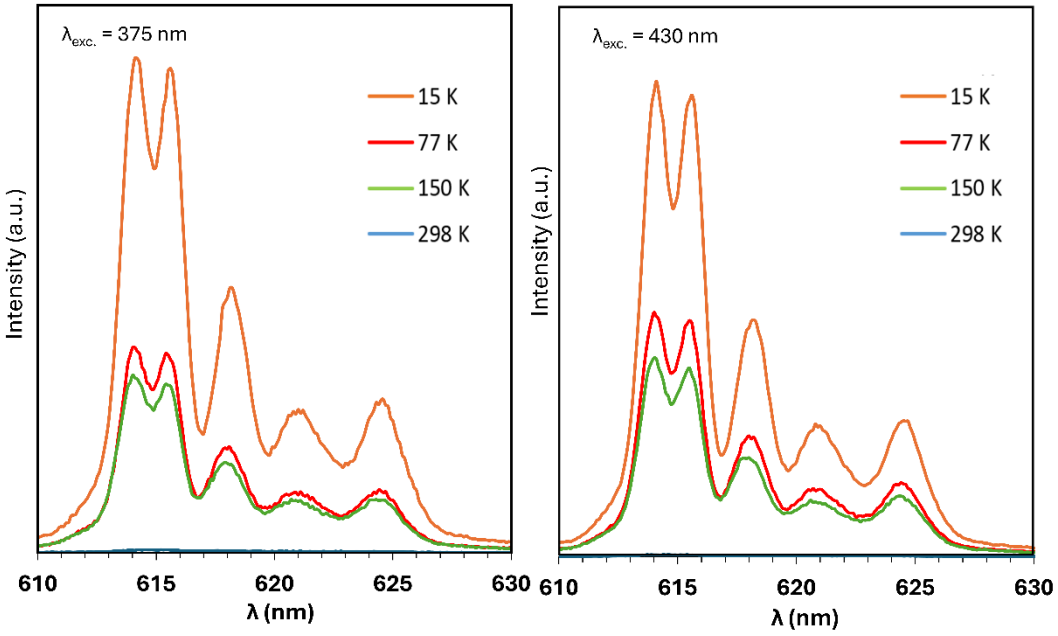

Figure S28. Thermal evolution of the most intense transition of **1_{Ge}-Eu** upon excitation at 375 and 420 nm.

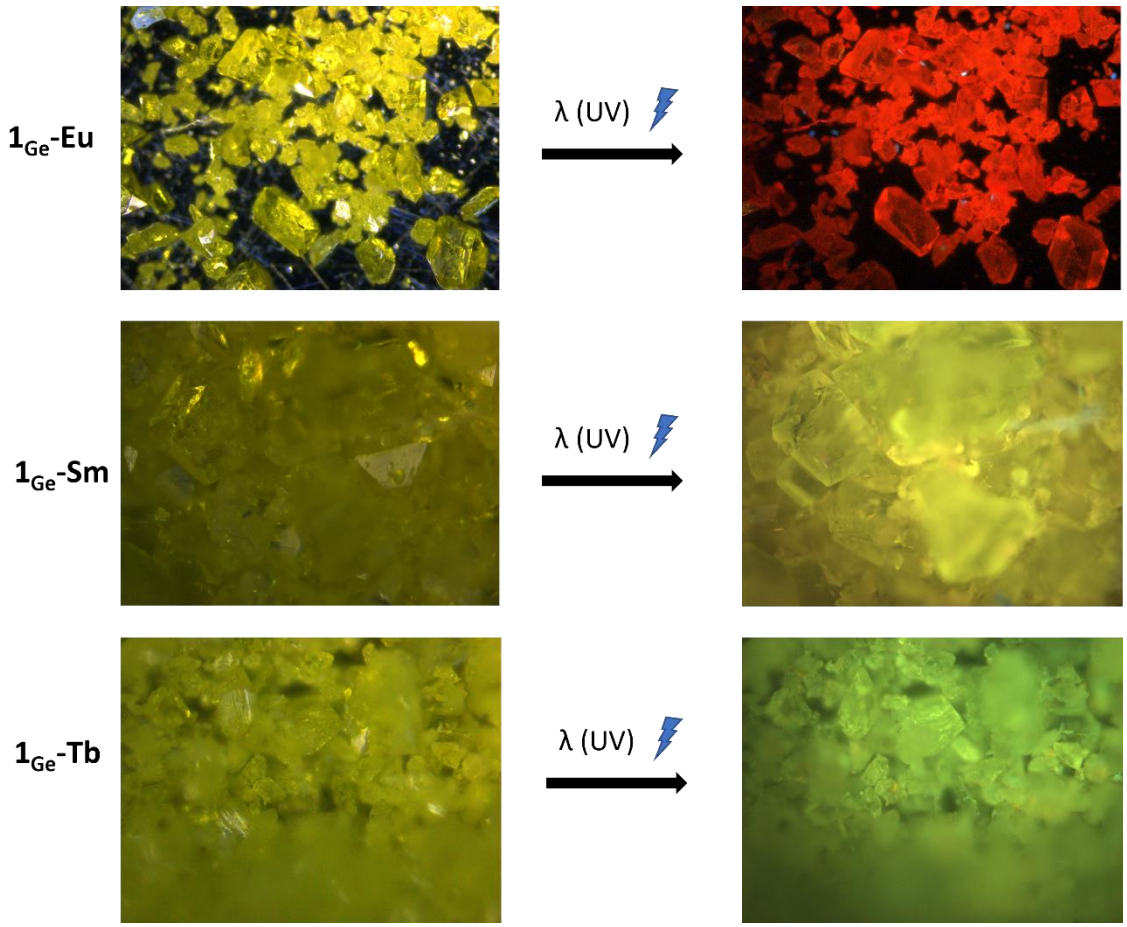

Figure S29. Left: Photographs of crystals of **1_{Ge}-Sm** (top), **1_{Ge}-Eu** (middle) and **1_{Ge}-Tb** (bottom) before irradiation with UV light. Right: photographs of the crystals after irradiation with UV light.

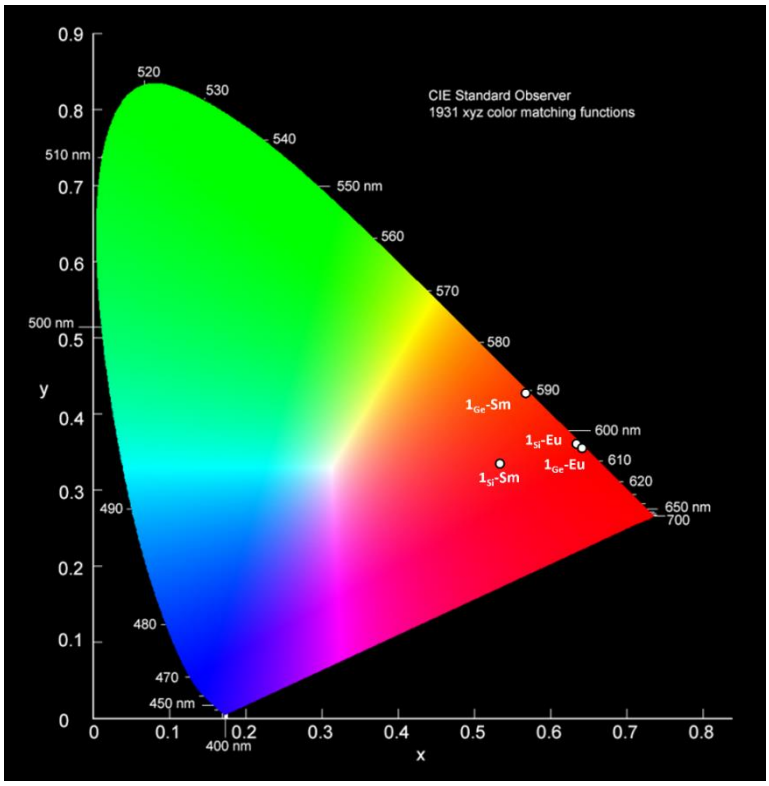

Figure S30. CIE 1931 x,y chromaticity coordinates as function of the emission wavelengths for compounds **1_x-Ln** (x = Ge, Si; Ln = Sm, Eu).

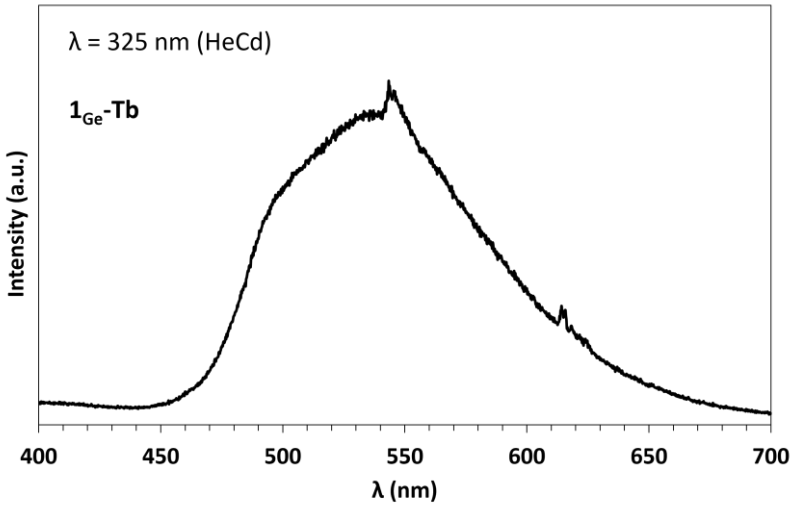

Figure S31. Solid state photoluminescence spectra for **1_{Ge}-Tb** recorded at 15 K and upon excitation at 325 nm.

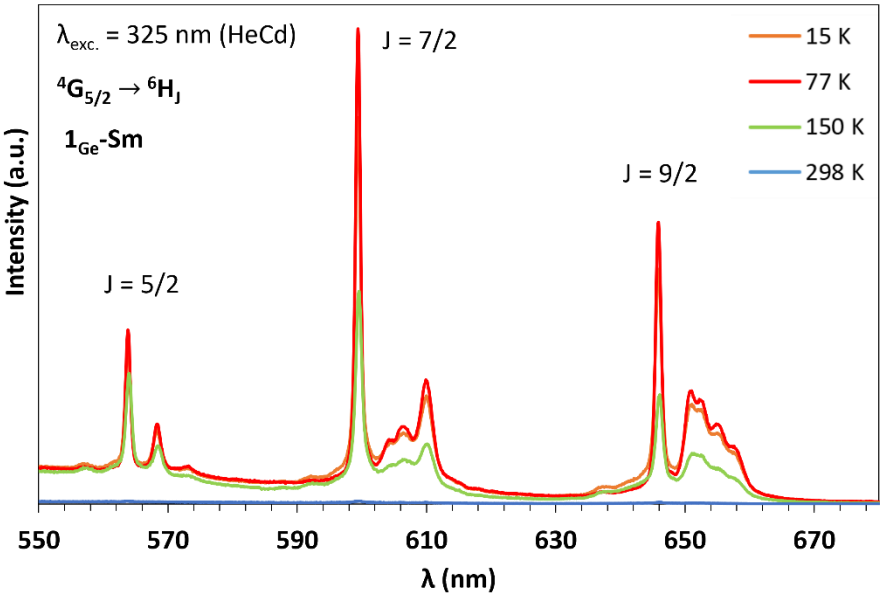

Figure S32. Thermal evolution of the solid-state photoluminescence spectrum of **1_{Ge}-Sm** recorded at 15, 77, 150 and 298 K upon excitation at 325 nm with the HeCd laser.

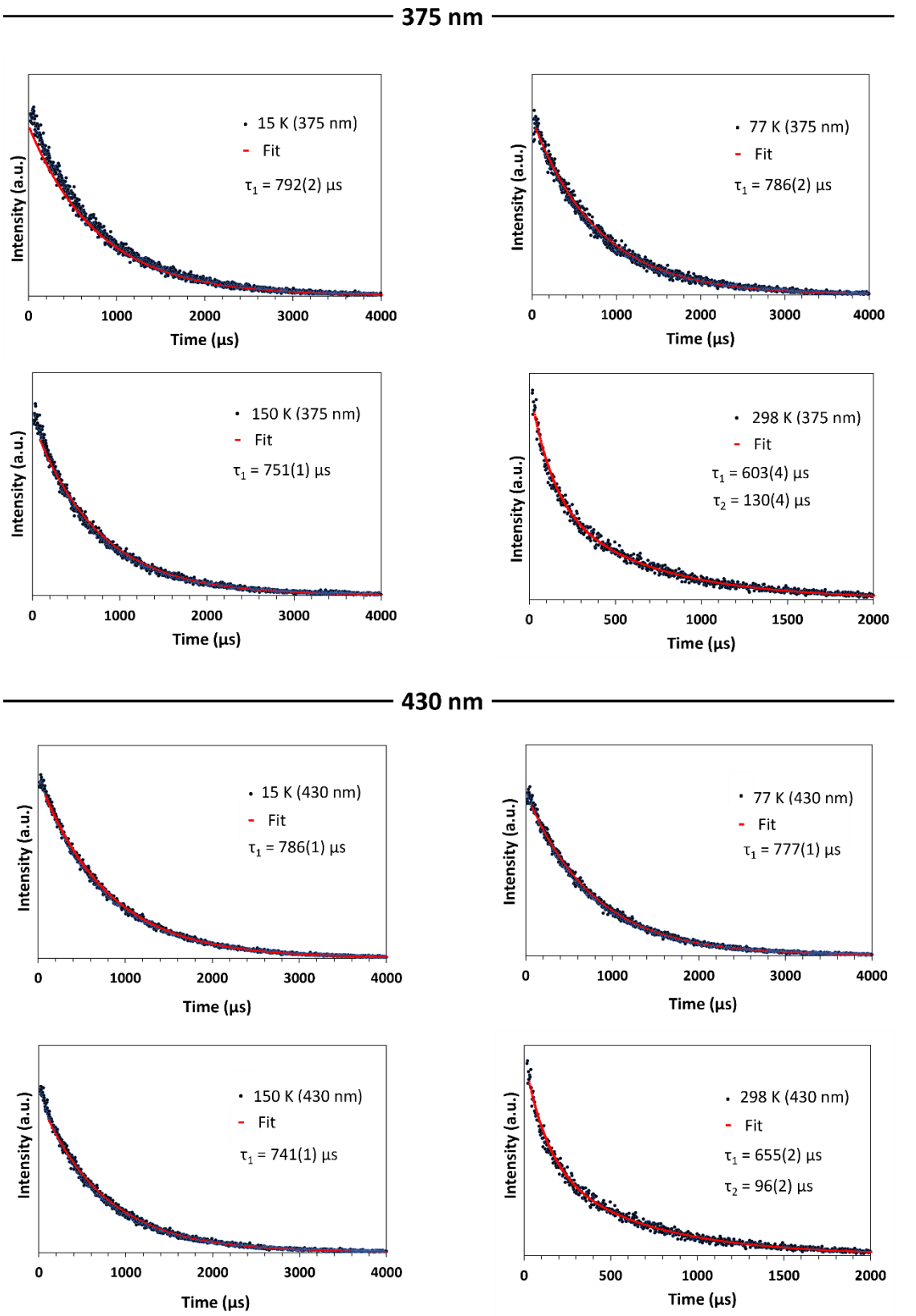

Figure S33. Luminescence decay curves for **1_{Ge}-Eu** at different temperatures upon excitation at 375 nm (top) and 430 (bottom).

Table S10. Luminescence lifetimes of **1_{Ge}-Eu** upon excitation at 375 nm and 430 nm at different temperatures.

T (K)	τ_1 (µs) / τ_2 (µs) (Exc. 375 nm)	τ_1 (µs) / τ_2 (µs) (Exc. 430 nm)
15	792(2)	786(1)
77	786(2)	777(1)
150	751(1)	741(1)
298[a]	603(4) / 130(4)	655(2) / 96(2)

[a] = $A_0 + A_1 \cdot \exp(-t/\tau_1) + A_2 \cdot \exp(-t/\tau_2)$

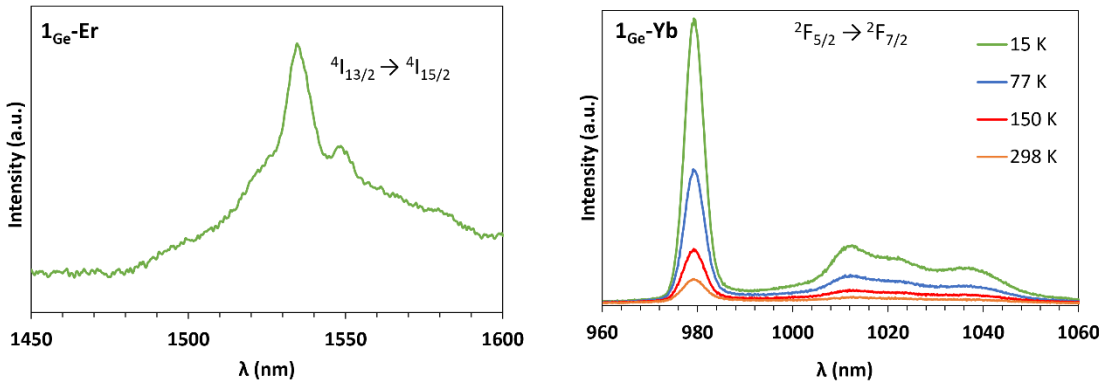

Figure S34. Solid state photoluminescence spectra for **1_{Ge}-Er** recorded at 15 K (left) and **1_{Ge}-Yb** recorded at different temperatures (right) upon excitation at 325 nm.

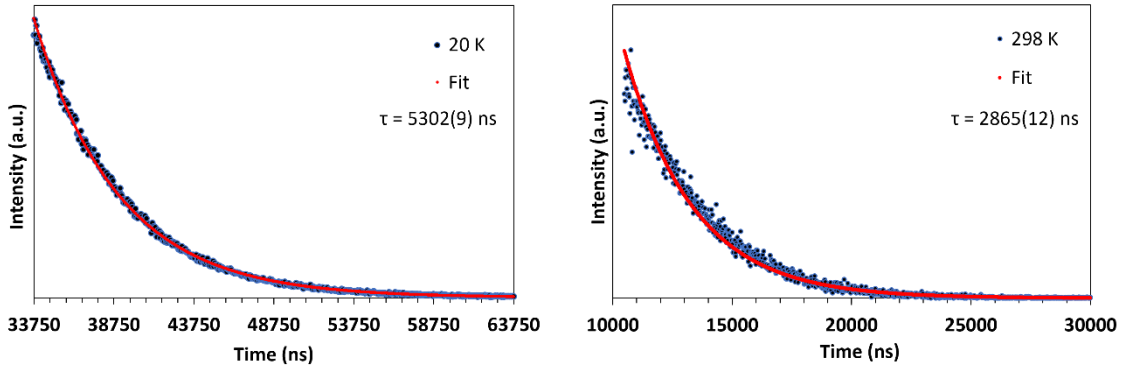

Figure S35. Luminescence decay curves for **1_{Ge}-Yb** at 20 K (left) and room temperature (right) upon excitation at 325 nm.

References

[1] A. Tézé and G. J. Heré, *Inorganic Synthesis*, John Wiley and Sons, New York, 1990.
[2] M. Yonemura, Y. Matsumura, H. Furutachi, M. Ohba, H. Okawa and D. E. Fenton, *Inorg. Chem.*, 1997, **36**, 2711–2717.
[3] T. Kudo, J. Oi, A. Kishimoto and M. Hiratani, *Mater. Res. Bull.*, 1991, **26**, 779–787.
[4] V. I. Spitsyn and V. K. Trunov, *Dokl. Chem.*, 1968, **183**, 978.
[5] *CrysAlisPro Software System*, version 171.37.34, Agilent Technologies UK Ltd, Oxford, UK, 2012.
[6] O. V. Dolomanov, L. J. Bourhis, R. J. Gildea, J. A. K. Howard and H. Puschmann, *J. Appl. Crystallogr.*, 2009, **42**, 339–341.
[7] G. M. Sheldrick, *Acta Crystallogr., Sect. C: Struct. Chem.*, 2015, **71**, 3–8.
[8] L. A. Spek, *Acta Crystallogr. Sect. D: Biol. Crystallogr.*, 2009, **D65**, 148–155.
[9] L. J. Farrugia, *J. Appl. Crystallogr.*, 1999, **32**, 837–838.
[10] D. C. Palmer, *Crystal Maker*, CrystalMaker Software Ltd, Oxford, UK, 2014.
[11] D. Casanova, M. Llunell, P. Alemany and S. Alvarez, *Chem. – Eur. J.*, 2005, **11**, 1479–1494.